

Laboratory 2 - Underdamped, Free/Driven Oscillator

Lizzy Jones
Due: April 18, 2023

Contents

1 Theory	1
1.1 Experimental Setup	1
1.2 Assumptions, Models and Free Body Diagrams	2
1.3 Derivation of the Equations of Motion	8
1.4 Solving for Analytical Solutions	13
1.4.1 Cases 1-4	13
1.4.2 Case 5	15
2 Results and Discussion	17
2.1 Finding the Spring Constant, k	17
2.2 Experimental Specifications	18
2.3 Experimental Results and FFT: Cases 1-4	19
2.4 Fitting the Data: Cases 1-4	20
2.5 Comparison of Analytical and Experimental Data	24
2.6 Discussion and Sources of Error: Cases 1-4	25
2.7 Results and Discussion: Case 5	27
3 Appendix	31
3.1 Data for Spring Force vs. Displacement	31
3.2 Plots of Analytical Prediction with Fitted Sinusoid	32
3.3 Code	34

1 Theory

1.1 Experimental Setup

In this experiment I analyze the motion of a pendulum system. The experimental setup consisted of a large metal cage with a roller bearing fixed to its top. An axle is placed inside the bearing so that it can spin with minimal friction. A pendulum rod is attached to this axle so that it swings as the axle spins. A white resin cylinder is attached near the base of the rod to help with data acquisition. An ultrasonic sensor is positioned on the side of the metal cage at the height of the resin cylinder; during data acquisition, it uses the color and reflections off the cylinder to determine the cylinder's horizontal displacement in inches [1]. The setup also includes a Pasco Mechanical Wave Driver (SF-9324), which oscillates horizontally in a sinusoidal motion, and its frequency can be set in 0.1Hz increments [1]. This is referred to as the "shaker" throughout this report. The data collected from the ultrasonic sensor was processed using LABVIEW software, measuring position vs. time in inches per second [1]. Figure 1 provides an image of the general setup.

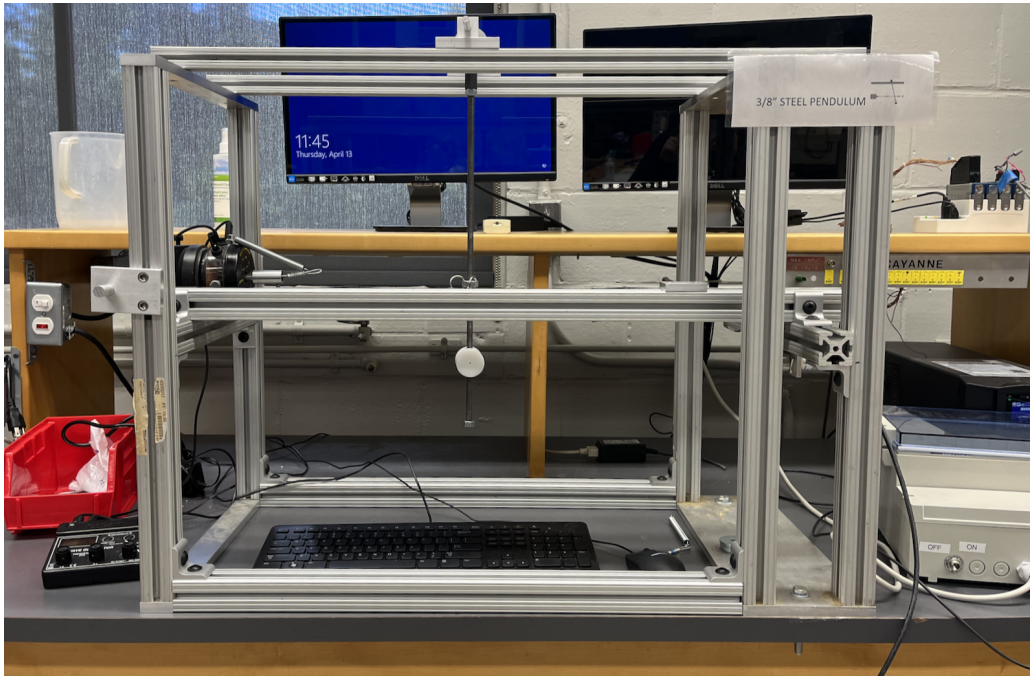


Figure 1: Setup of Pendulum

Our system used a 3/8 inch steel pendulum rod, but rods were available in various lengths, materials, and sizes. Regardless, all systems operate on the same principle. An image of the rod we used, including the white resin cylinder is included in Figure 2. Specifications about our particular system are included in Table 6, whereas this section works to derive equations of motion for any general case.

We gathered data for various different configurations of the pendulum setup pictured above. In total, five modifications of the system were analyzed. Each of these systems are described below:

Case 1: The first case was a simple pendulum. The pendulum rod was attached to a roller bearing at a fixed point on the top of the metal cage. No extra mass was added to this system beyond the mass of the pendulum itself. The pendulum was released from a small angle ($\approx 15^\circ$)



Figure 2: Pendulum Rod with White Resin Cylinder

from the vertical)

Case 2: The second case was the same as the first, but we added a large mass to the system by attaching ten metal washers and a nut just below the white resin cylinder.

Case 3: The third case consisted of a pendulum rod with a small attached mass. We achieved this by removing five washers from case 2, leaving five washers and the nut on the rod. Case 3 also includes springs attached on either side of the rod, at the adjustable metal collar visible in Figure 2. The other side of the springs were fixed on opposite sides of the cage.

Case 4: The fourth case was the same as case 3, except there were no springs attached. Instead, the pendulum could swing freely (as in cases 1 and 2) with an added mass of 5 washer and a nut.

Case 5: The final case was similar to case 3 in that included an extra mass of five washer and a nut as well as springs attached just above the resin cylinder. Instead of both springs being fixed to the cage, however, one of the springs was attached to the shaker.

1.2 Assumptions, Models and Free Body Diagrams

In modelling the five systems, we made several simplifying assumptions so that it was possible to describe the system with mathematical expressions. The simplifications and assumptions made to the general system are as follows:

First it is assumed that in all cases, the pendulum is undergoing small angle oscillation. A corollary of this assumption is that the displacement of the pendulum at the location of measurement (eg the white resin cylinder) is purely horizontal. This also applies to the springs; they are assumed to produce a force purely in the horizontal direction and have no vertical component. This assumption is valid because we released the pendulum from a maximum angle of 15° from the vertical, for which the small angle approximation $\sin \theta = \theta$ has an error of only 1.16 %.

It is assumed that roller bearing created a damping torque in the direction opposite motion, and that this torque could be modelled linearly. I also assumed that damping occurs only at the pin, neglecting any other damping forces present such as air drag. This assumption is reasonable

because the pendulum was relatively thin and was not moving extremely quickly, so air drag likely did not have a large effect on pendulum motion.

Additionally, the rod is assumed to be long and slender. I neglected the volume of the white resin cylinder and assumed its mass was distributed evenly along the length of the rod. This is a reasonable assumption because the weight of the resin piece is much smaller than that of the rod, which was 3/8 inch solid steel, so its effect on the distribution of mass was negligible. The weights of both elements are included in Table 6. Furthermore, we added mass to the system in the form of washer and a nut fastened below the resin cylinder in cases 2, 3, 4, and 5. This mass was approximated to be a point mass. Because the entire height of the assembly was less than 2cm, this was a reasonable assumption. Gravity is assumed to act directly downward at a magnitude of 9.81 m/s^2 .

Using these assumptions, I created a mathematical model for each of the five cases. Case 5 is the most complex, and all of the various cases are constituent parts of that case. In addition to the assumptions and simplifications stated above, I also made several assumptions specific to each case. These are discussed alongside the corresponding models, which are presented below.

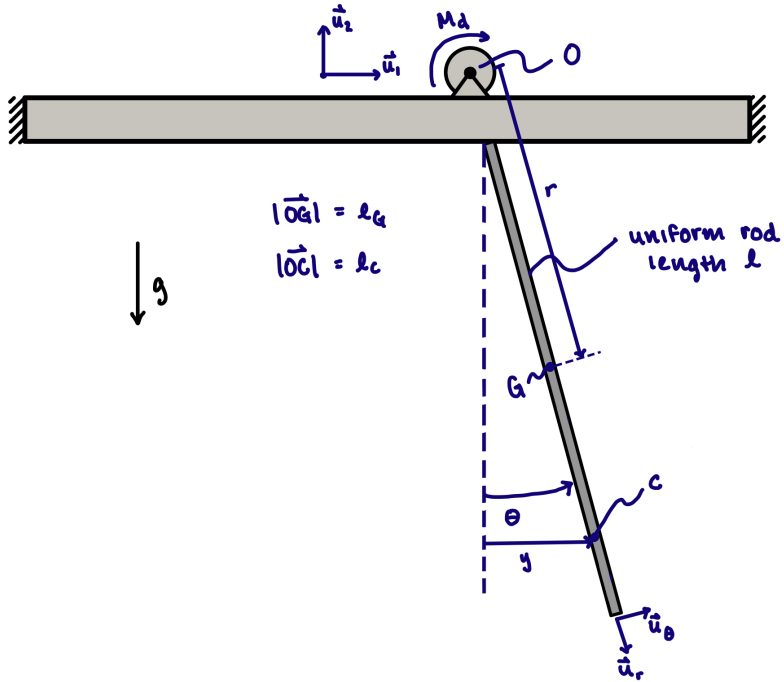


Figure 3: Mathematical Model of Case 1, adapted from lecture notes [2]

Figure 3 shows a model of case 1, where $g = \text{gravity}$, O is the inertially fixed point around which the pendulum rotates, M_d is a damping torque applied at pin O , G is the center of mass of the rod, l_g is the rod's full length, C is the center of mass of the resin cylinder, and l_c is the distance from point O to point C . Note that the mass of the cylinder is neglected, but the location of this point is critical because it is the point at which the ultrasonic sensor took data. The rod has mass m_l . I chose two reference frames for this system. The first is the Cartesian frame denoted by \vec{u}_1 which points to the right and \vec{u}_2 which points upward. I also used a polar reference frame, where \vec{u}_r

points away from O in the direction of the rod and \vec{u}_θ points 90 degrees counterclockwise from \vec{u}_r . The coordinate variables used are r , which spans from point O to point G , θ which measures the counterclockwise angular displacement of the pendulum from the vertical, and y , which measures the horizontal displacement of the resin cylinder. In all other systems, these variables are also used and have the same significance as in case 1.

Case 1 one of the simplest models because it includes only a rod which is pinned at point O . M_d is an unknown damping torque which I have chosen to model as $M_d = b\dot{\theta}$ where b is a damping coefficient. M_d acts in the direction that impedes motion and varies linearly with angular speed of the pendulum. Note that the resin cylinder is omitted from the drawing because my model neglects its mass and volume as explained above. Also, although this is a 3 dimensional physical system, I have chosen to model it in two dimensions. This is because the system is pinned at the top, restricting motion in the \vec{u}_1 and \vec{u}_2 directions. Because of this simplification, it has only one degree of freedom and moves only along the $\vec{u}_1\vec{u}_2$ plane, so it is appropriate to model in two dimensions. This is true of all five models.

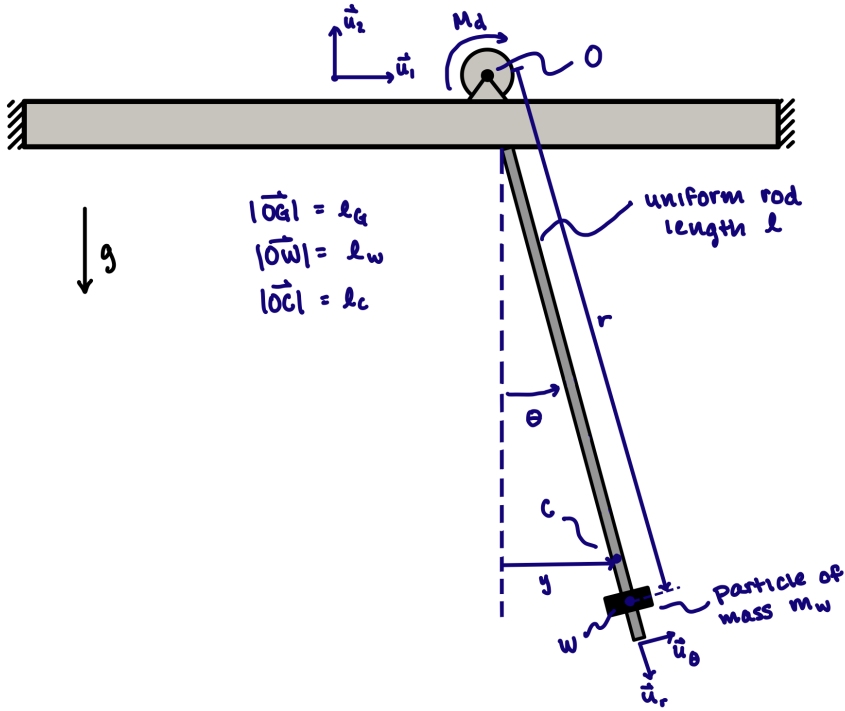


Figure 4: Mathematical Model of Case 2, adapted from lecture notes [2]

In the physical system for case 2, we added a mass toward the end of the rod. In my model as depicted in Figure 4, this is represented as a point particle of mass m_w positioned at point W , fixed on the rod. The same assumptions from Case 1 about the damping torque M_d apply in Case 2. For this model, it was assumed that the mass of the rod is negligible, and only the added mass is considered in calculations. This is reasonable because the added mass was chosen to be heavy enough that it would overpower the effects of the rod (for specific information on each component's mass, see Tables 6 and 7). The center of mass G of the system is therefore located at point W . For this reason, the position vector r is drawn from point O to point W .

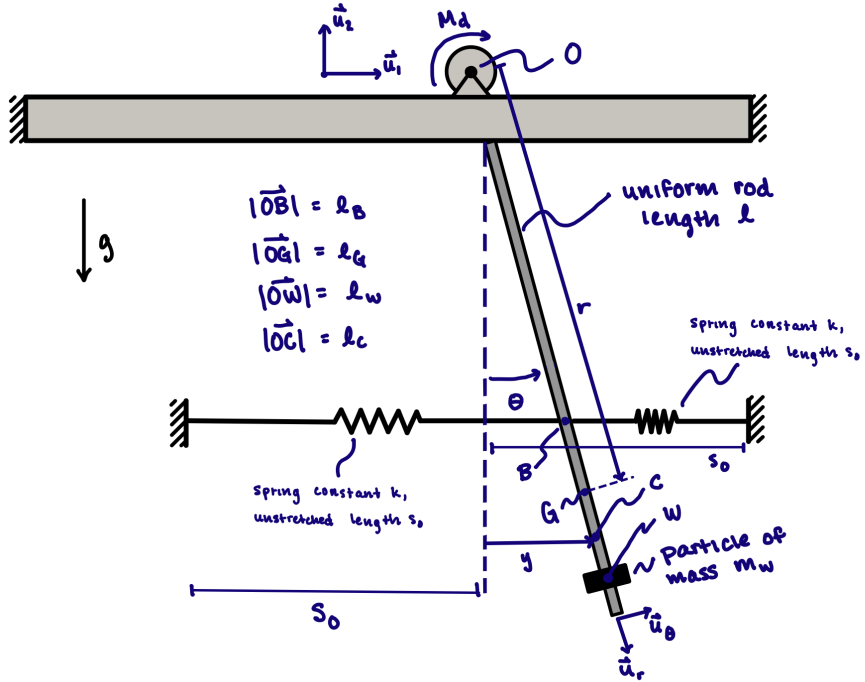


Figure 5: Mathematical Model of Case 3, adapted from lecture notes [2]

For case 3, the value of the added mass was decreased and springs were added to the system, as is visible in Figure 5. In this system, the springs have spring constant k , natural length s_o and are assumed to be unstretched when $\theta = 0$. The springs are attached to the rod at point B . The distance from point O to point B is l_b . The other end of the springs are assumed to be fixed to stationary supports at the same height as point B on the rod. Additionally, because I am assuming small angle approximation, point B is assumed to move only horizontally with no vertical component. As a result, the spring forces on the rod are strictly horizontal. The spring forces are assumed to be equal in compression and tension so that both springs provide the same magnitude force on the rod at all times. This is a simplification to the system because in reality, the springs are stronger in tension than in compression [1]. The diameter of the rod is also neglected, the displacement of each spring is assumed to be equal (but in opposite directions) at any time.

Unlike in case 2, case 3 does not assume the rod is massless. Instead, the rod has mass m_r and length l_r . The added mass is again modelled as a point particle of mass m_w at point W on the rod. The mass is assumed to be fixed in place on the rod. Therefore, the center of mass G is fixed on the rod as well and is positioned between the center of mass of the rod and the point mass. In the coordinate vector r is drawn from point O to point G .

Case 4 is presented in Figure 6. This case is the same as case 3, except there are no springs attached. Therefore, all the same assumptions not related to the springs apply to this case as well. Note in particular that the system is again modelled as a point particle of mass m_w fixed to a long slender rod of mass m_r .

Finally, case 5 is presented in Figure 7. This case is exactly the same as case 3, except has an additional shaker component which is fixed to the end of one of the springs. It shakes back

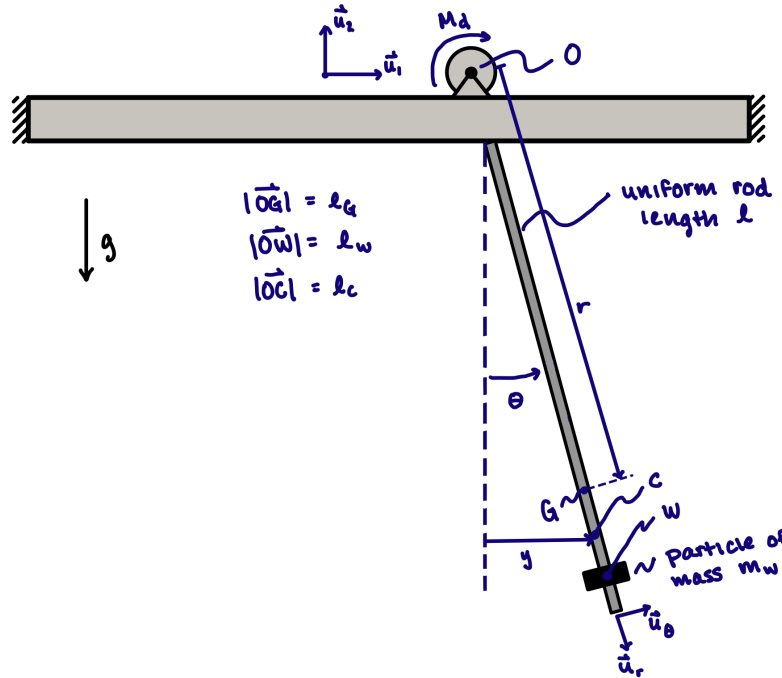


Figure 6: Mathematical Model of Case 4, adapted from lecture notes [2]

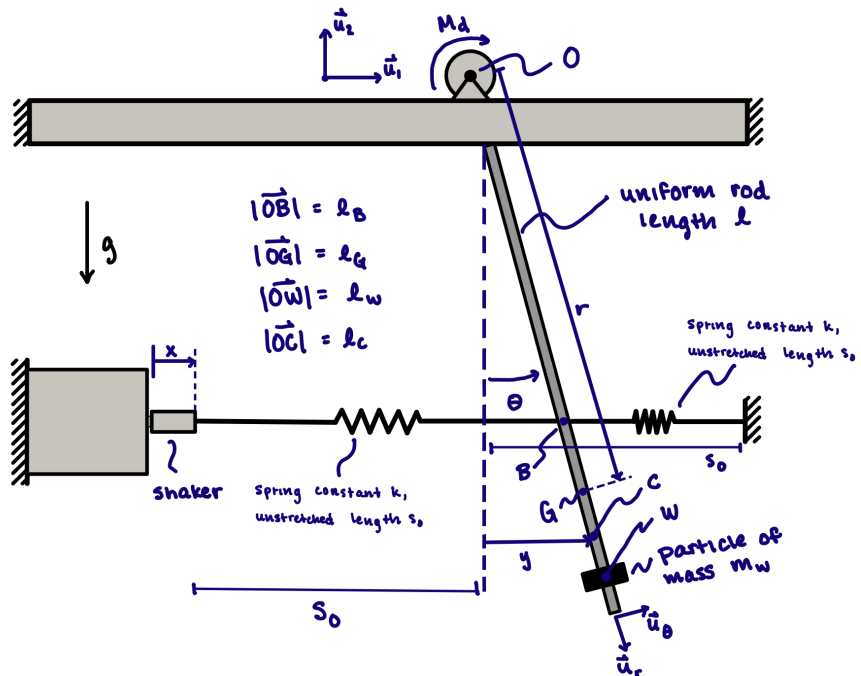


Figure 7: Mathematical Model of Case 5, adapted from lecture notes [2]

and forth in a purely horizontal sinusoidal motion, as noted previously. Since the other side of the spring is attached to the rod, the motion of the shaker affects the net displacement of that spring and therefore the force it imparts on the rod. The displacement of the shaker from its initial position is labelled by the coordinate variable x . The motion of the shaker is sinusoidal in time, where the amplitude of its motion is x_o and frequency is ω_o . Therefore, the motion of the shaker, $x(t)$, can be described as $x(t) = x_o \sin \omega_o t$.

These models can be used to make free body diagrams of each setup. Though all systems are similar, each case has a unique free body diagram based on the modelling choices made. Cases 1, 2 and 4 are considered together first in Figure 11, as they do not include springs. Cases 3 and 5 are considered in Figure 14 because they both include spring forces.

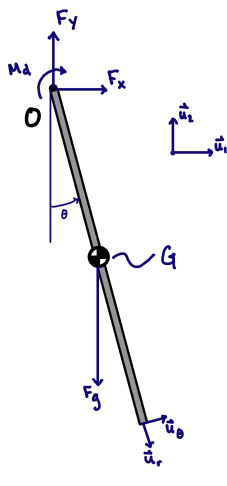


Figure 8: Case 1

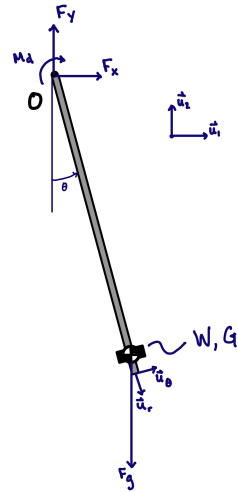


Figure 9: Case 2

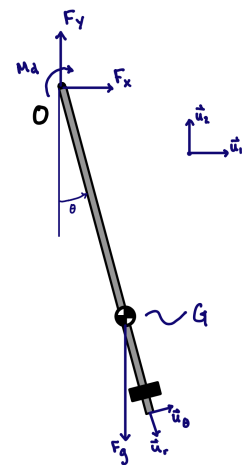


Figure 10: Case 4

Figure 11: Free Body Diagrams: Cases 1, 2, and 4

In all cases, the rod experiences gravity acting on the center of mass. This force is depicted as F_g in the free body diagrams and acts straight downward in the $-\vec{u}_2$ direction. The location of the center of mass varies by case, so the specific point of application of the gravitational force is not the same in all cases. For instance, in Case 1, gravity acts at the center of the rod; in case 2, gravity acts at point W at the position of the point mass; in case 4, gravity acts between the center of the rod and point W , at point G .

All five systems also include two reaction forces at the pin at point O . These are constraint forces which are modelled in the \vec{u}_1 and \vec{u}_2 directions, respectively. They restrict motion of the rod at point O in their respective directions. The last element of the free body diagram in cases 1, 2, and 4 is the torque M_d which is applied at the pin O . This torque acts in the $-\vec{u}_3$ direction, where $\vec{u}_3 = \vec{u}_1 \times \vec{u}_2$. The magnitude of M_d is $b\dot{\theta}$, where b is a damping coefficient as described in the previous section.

Cases 3 and 5 contain all the same elements as cases 1, 2, and 4. Additionally, the springs are attached to the rod in these cases, so their force is also included in the free body diagram. In analyzing this section, the linearization of the motion for small θ is used. Since the springs are assumed to only provide horizontal force, they can be expressed in the direction \vec{u}_1 rather than in terms of \vec{u}_r and \vec{u}_θ . As defined in our assumptions, the springs in cases 3 and 5 are assumed to be at equilibrium when $\theta = 0$. They are attached to the pendulum at point B (distance l_b from the origin as labelled in Figure 5), so their horizontal displacement from $\theta = 0$ at any time is $l_b \sin \theta$.

Note that, as drawn in the Free Body Diagram in Figure 14, the pendulum experiences the force of both springs in the same direction at any given time because one spring is in compression and the other is in tension.

For case 3, the springs each have a force of magnitude $F_s = -kd$ according to Hooke's Law, where k is the spring constant and d is the displacement of the spring from equilibrium. The negative sign is present because the spring force is restorative, so it acts to decrease θ . The rod is assumed to have negligible diameter, so the displacement of both springs is assumed to be the same value ($l_b \sin \theta$) as derived above. Since both springs impart an equal force on the rod, their total effect is $2F_s$ in the $-\vec{u}_1$ direction.

In case 5, the right-hand spring is unaffected by the addition of the shaker and has a force $\vec{F}_{s,right} = -kl_b \sin \theta \vec{u}_1$. The left-hand spring is attached to the shaker, which has a varying displacement of $x(t) = x_o \sin \omega_o t$, where x_o is the amplitude of the shaker's motion, ω_o is its frequency, and t is time as explained in the discussion on the mathematical model for case 5. Therefore, the left-hand spring has a varying displacement of $(l_b \sin \theta - x) \vec{u}_1$ from its equilibrium (see Figure 7). Using Hooke's law, the total force on the rod from the left spring is $\vec{F}_{s,left} = -k(l_b \sin \theta - x) \vec{u}_1$. The total force of both springs in case 5 is found by adding the $\vec{F}_{s,left}$ and $\vec{F}_{s,right}$ terms together which is displayed as two separate vectors in Figure 13:

$$\vec{F}_{s,left} + \vec{F}_{s,right} = -k(2l_b \sin \theta - x_o \sin \omega_o t) \vec{u}_1 \quad (1)$$

Force due to springs in Case 3 can be expressed using this same expression where x_o , the displacement of the shaker, is zero.

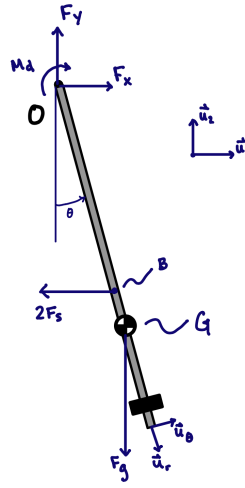


Figure 12: Case 3

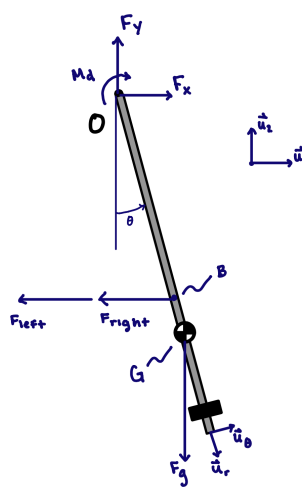


Figure 13: Case 5

Figure 14: Free Body Diagrams: Cases 3 and 5

1.3 Derivation of the Equations of Motion

Using the models and free body diagrams in the section above, it is possible to derive equations of motion for each system using Euler's laws or Lagrange's method. I chose to use Lagrange's method because I prefer to work with scalars rather than vectors in complex systems. Before beginning this process, though, it is helpful to derive expressions for l_g (the distance from O to G) and I_o (the

moment of inertia of the system about point O) so that they may be used in the Lagrange method derivation.

The distance l_G can be found by taking the absolute value of the coordinate variable $\vec{r}_{G/O}$ which is illustrated in Figures 3 to 7 and defines the distance from point O to the center of mass of the pendulum system, G . Using the assumptions defined, the pendulum system can be treated as a rigid body with a slender uniform rod of length l_r and mass m_r connected to a point mass at position l_w away from O along the rod and mass m_w . Because the the rod is assumed to be uniform, its center of mass is located at $\frac{1}{2}l_r$ from either end. The position of the center of mass of a rigid body is found as a weighted average of the masses of all constituent components, which allows us to quantify l_g as follows:

$$l_G = |\vec{r}_{G/O}| \quad (2)$$

$$\vec{r}_{G/O} = r\vec{u}_r \quad (3)$$

$$\vec{r}_{G/O} = \frac{\frac{1}{2}l_r m_r + l_w m_w}{m_r + m_w} \vec{u}_r \quad (4)$$

$$l_g = \frac{\frac{1}{2}l_r m_r + l_w m_w}{m_r + m_w} \quad (5)$$

These values vary by case, but Equation 5 is general and applies to each case. For case 1, $m_w = 0$, so Equation 5 reduces to $l_g = \frac{1}{2}l_r$. Similarly for case 2, $m_r = 0$ so 5 reduces to $l_g = l_w$. The expression for each case is listed specifically in Table 1. The exact value of l_G for each case can be determined numerically based on system specifications and is provided in Table 7.

To find I_O , I can use the parallel axis theorem, where I_G is the moment of inertia of a body about its center of mass, m is its mass, and l_G is the distance between points O and G [3]:

$$I_O = I_G + ml_G^2 \quad (6)$$

This formula can be applied to each element of the rigid body then added together to find the total system's moment of inertia about point O . The procedure follows in Equations 7 to 12, where $I_{O,rod}$ and $I_{G,rod}$ are the moments of inertia of the rod about points O and G respectively and $I_{O,mass}$ and $I_{G,mass}$ are the moments of inertia of the point mass about points O and G respectively. Note that the moment of inertia of a slender rod of mass m and length l about its center of mass is defined to be $\frac{1}{12}ml^2$ whereas the moment of inertia of a point mass about its center of mass is zero.

$$I_O = I_{O,rod} + I_{O,mass} \quad (7)$$

$$I_{O,rod} = I_{G,rod} + \frac{1}{4}m_r l_r^2 \quad (8)$$

$$= \frac{1}{3}m_r l_r^2 \quad (9)$$

$$I_{O,mass} = I_{G,mass} + m_w l_w^2 \quad (10)$$

$$= m_w l_w^2 \quad (11)$$

$$I_O = \frac{1}{3}m_r l_r^2 + m_w l_w^2 \quad (12)$$

This again applies to all cases. For case 1, $m_w = 0$ so Equation 12 reduces to $I_O = \frac{1}{3}m_r l_r^2$. For case 2, $m_l = 0$ so Equation 12 reduces to $I_O = m_w l_w^2$.

The simplified expressions for l_g and I_o are summarized in Table 1 below. The values of each variable vary by case and are summarized in Table 7.

Table 1: Expressions for l_g and I_o for Each Case

Case	l_g (Distance from O to G)	I_o (Moment of Inertia about O)
1	$\frac{1}{2}l_r$	$\frac{1}{3}m_l l_r^2$
2	l_w	$m_w l_w^2$
3, 4, 5	$\frac{m_w l_w + \frac{1}{2}m_r l_r}{m_w + m_r}$	$\frac{1}{3}m_r l_r^2 + m_w l_w^2$

With these values defined, I can begin Lagrange's method. The first step is to define the generalized coordinate(s) q_i for the system. For this system, there is one degree of freedom: the pin at the top constrains the \vec{u}_1 and \vec{u}_2 directions as the pendulum swings about the \vec{u}_3 axis ($\vec{u}_1 \times \vec{u}_2 = \vec{u}_3$). The motion can therefore be described completely using only one generalized coordinate variable. I chose to use $q_1 = \theta$ because this is the variable used to describe motion in my mathematical models and free body diagrams.

Then, I defined energies of the system, kinetic energy T_o and potential energy U_o at an arbitrary state s_1 . The rod rotates around an inertially fixed point O , so the kinetic energy can be expressed using the fixed point rotation simplification [3]. This simplification uses the moment of inertia of the entire pendulum about the origin I_o and the angular velocity of the body $\omega = \dot{\theta}$ to define the kinetic energy as follows:

$$T_o = \frac{1}{2}I_o\omega^2 \quad (13)$$

$$= \frac{1}{2}I_o\dot{\theta}^2 \quad (14)$$

Given l_g and I_o as defined in equations 5 and 12 respectively, it is possible to solve numerically for the kinetic energy of the rod, T_o using Equation 14. Again, this formula can be applied to any of the five cases by varying the numerical values of l_g and I_o based on the system parameters for that case.

The next step is to find the potential energy of a system at an arbitrary state, U_o . This term consists of all sources of conservative work, which includes gravity in all five cases as well as the spring force in cases 3 and 5. Potential energy of a rigid body due to gravity, U_{grav} is given by $U_{grav} = mgh_G$ where m is the mass of the body, g is gravitational acceleration (9.81 m/s^2) and h_G is the height of the body's center of mass measured upward (the \vec{u}_2 direction) from point O [4]. For the pendulum system in each case, the potential energy due to gravity is as follows, using m_b as the mass of the entire body:

$$U_{grav} = -(m_r + m_w) \cdot g \cdot l_g \cos \theta \quad (15)$$

$$= -m_b g l_g \cos \theta \quad (16)$$

The $\cos \theta$ term is included to account for just the vertical component of the length l_g , which represents the negative height of point G at that angle. This can be easily seen in the free body diagrams for each case in Figures 11 and 14.

Potential energy due to a spring is defined generally as $U_{spring} = \frac{1}{2}kd^2$ where k is the spring constant of the spring and d is the displacement of the spring from its equilibrium point. Using the relationship $d = l_b \sin \theta - x_o \sin \omega_o t$ for the left-hand spring and $d = l_b \sin \theta$ for the right-hand spring for cases 3 and 5 as derived in Equation 1, the total potential energy is as follows:

$$U_{springs} = \frac{1}{2}k(l_b \sin \theta)^2 + \frac{1}{2}k(l_b \sin \theta - x_o \sin \omega_o t)^2 \quad (17)$$

$$= \frac{1}{2}k(l_b \sin \theta)^2 + \frac{1}{2}k(l_b \sin \theta - x_o \sin \omega_o t)^2 \quad (18)$$

This applies to both cases 5 and 3, where the amplitude shaker displacement x_o is zero in case 3.

For cases 1, 2, and 4, the total potential energy U_o is equal to U_{grav} . However, in cases 3 and 5, it is necessary to incorporate the springs. For these systems, the total potential energy can be found by adding together the gravitation and spring potential energies:

$$U_o = U_{grav} + U_{spring} \quad (19)$$

$$U_o = -m_b \cdot g \cdot l_g \cos \theta + \frac{1}{2}k(l_b \sin \theta)^2 + \frac{1}{2}k(l_b \sin \theta - x_o \sin \omega_o t)^2 \quad (20)$$

Table 2 summarizes the kinetic and potential energies for each system below:

Table 2: Expressions for Kinetic Energy T_o and Potential Energy U_o for Each Case

Case	Kinetic Energy (T_o)	Potential Energy (U_o)
1, 2, 4	$\frac{1}{2}I_o\dot{\theta}^2$	$-m_b \cdot g \cdot l_g \cos \theta$
3, 5	$\frac{1}{2}I_o\dot{\theta}^2$	$-m_b \cdot g \cdot l_g \cos \theta + \frac{1}{2}k(l_b \sin \theta)^2 + \frac{1}{2}k(l_b \sin \theta - x_o \sin \omega_o t)^2$

The Lagrangian is defined using these system energies as the following:

$$L = T_o - U_o \quad (21)$$

Therefore, the Lagrangian for each case is as follows, with L_i representing the Lagrangian for case i :

$$L_{1,2,4} = \frac{1}{2}I_o\dot{\theta}^2 + m_b \cdot g \cdot l_g \cos \theta \quad (22)$$

$$L_{3,5} = \frac{1}{2}I_o\dot{\theta}^2 + m_b \cdot g \cdot l_g \cos \theta - \frac{1}{2}k((l_b \sin \theta)^2 + (l_b \sin \theta - x_o \sin \omega_o t)^2) \quad (23)$$

The next step is to define the generalized force coordinate, Q_1 . This coordinate is defined as follows, where \vec{F}_j represents a nonconservative, nonconstraint external force, \vec{r}_j is the position vector of the point at which the force F_j acts, \vec{M}_k is an externally applied torque, and $\vec{\omega}$ is the angular velocity of the body.

$$Q_1 = \sum_{j=1}^m \vec{F}_j \cdot \frac{\partial \vec{r}_j}{\partial q_1} + \sum_{k=1}^n \vec{M}_k \cdot \frac{\partial \vec{\omega}}{\partial \dot{q}_1} \quad (24)$$

Again, this term varies by case based on the specific system parameters. Based on the free body diagrams in Figure 11, the only forces acting on the rod in cases 1, 2, and 4 are gravity, $-F_g \vec{u}_2$, and the reaction forces at the pin, $F_x \vec{u}_1$ and $F_y \vec{u}_2$. Gravity is conservative, so it does not contribute to Q_1 as an \vec{F}_j term. Similarly, the reaction forces at the pin are constraint forces, so they do not contribute to Q_1 either. (Note that even if they were nonconservative, they still would not contribute because the position vectors \vec{r}_x and \vec{r}_y are zero.)

Using the free body diagram in Figure 14 to analyze cases 3 and 5, the systems have all the forces described above as well as a spring force. Like gravity and the reaction forces at the pin, the spring force does not contribute to Q_1 because it is a conservative force. Thus, the first term of Q_1 in Equation 24 is zero since we neglected nonconservative forces like air drag. In all four cases, however, there is a nonzero moment \vec{M} due to friction at the pin. As detailed in the assumptions for the model, this moment was taken to vary linearly with angular speed $\dot{\theta}$ based on a constant drag coefficient b . The moment acts opposite the direction of motion, so it can be written as $\vec{M} = -b\dot{\theta}\vec{u}_3$.

Therefore, for all cases using $\vec{\omega} = \dot{\theta}\vec{u}_3$:

$$Q_1 = 0 + \vec{M}_d \cdot \frac{\partial \vec{\omega}}{\partial \dot{q}_1} \quad (25)$$

$$= -b\dot{\theta}\vec{u}_3 \cdot \frac{\partial \dot{\theta}\vec{u}_3}{\partial \dot{\theta}} \quad (26)$$

$$= -b\dot{\theta}\vec{u}_3 \cdot \vec{u}_3 \quad (27)$$

$$Q_1 = -b\dot{\theta} \quad (28)$$

Lagrange's method states that Q_1 can also be found in the following way:

$$Q_1 = \frac{d}{dt} \left(\frac{\partial L}{\partial \dot{q}_1} \right) - \frac{\partial L}{\partial q_1} = \frac{d}{dt} \left(\frac{\partial L}{\partial \dot{\theta}} \right) - \frac{\partial L}{\partial \theta} \quad (29)$$

Using the value of the Lagrangian $L_{1,2,4}$ for cases 1, 2, and 4 in equation 22, Equation 29 simplifies to the following:

$$Q_1 = \frac{d}{dt} \left(\frac{\partial \left(\frac{1}{2} I_o \dot{\theta}^2 + m_b \cdot g \cdot l_g \cos \theta \right)}{\partial \dot{\theta}} \right) - \frac{\partial \left(\frac{1}{2} I_o \dot{\theta}^2 + m_b \cdot g \cdot l_g \cos \theta \right)}{\partial \theta} \quad (30)$$

$$= I_o \ddot{\theta} + l_g m_b g \sin \theta \quad (31)$$

For cases 3 and 5 using Equation 23 for $L_{3,5}$:

$$Q_1 = \frac{d}{dt} \left(\frac{\partial L_{3,5}}{\partial \dot{\theta}} \right) - \frac{\partial L_{3,5}}{\partial \theta} \quad (32)$$

$$= I_o \ddot{\theta} + l_g m_b g \sin \theta + 2k l_b^2 \sin \theta \cos \theta - k x_o \sin \omega_o t \cos \theta l_b \quad (33)$$

For each case, Q_1 solved for in Equation 28 can be set equal to Q_1 in equations 31 and 33. For cases 1, 2, and 4, the following relationship results, combining Equations 28 and 31:

$$-b\dot{\theta} = I_o \ddot{\theta} + l_g m_b g \sin \theta \quad (34)$$

For cases 3 and 5, combining equations 28 and 33 yields:

$$k l_b x_o \sin \omega_o t \cos \theta - b\dot{\theta} = I_o \ddot{\theta} + l_g m_b g \sin \theta + 2k l_b^2 \sin \theta \cos \theta \quad (35)$$

Table 3: Equations of Motion for Cases 1-5

Case	Equation of Motion
1	$0 = I_o \ddot{\theta} + b\dot{\theta} + l_g m_b g \sin \theta$ where $l_g m_b = \frac{1}{2} l_r m_r$
2	$0 = I_o \ddot{\theta} + b\dot{\theta} + l_g m_b g \sin \theta$ where $l_g m_b = l_w m_w$
3	$0 = I_o \ddot{\theta} + b\dot{\theta} + l_g m_b g \sin \theta + 2k l_b^2 \sin \theta \cos \theta$
4	$0 = I_o \ddot{\theta} + b\dot{\theta} + l_g m_b g \sin \theta$
5	$kl_b \cos \theta x_o \sin \omega_o t = I_o \ddot{\theta} + b\dot{\theta} + l_g m_b g \sin \theta + 2k l_b^2 \sin \theta \cos \theta$

Simplifying this in each case yields the following equations of motion for each case, using $x_o = 0$ for case 3 (as discussed above): Where expressions for I_o and l_g for each case can be found in Table 1. Experimental values for these variables are based on system specifications and can be found in Tables 7 and 6.

1.4 Solving for Analytical Solutions

1.4.1 Cases 1-4

Given the equations of motion in Table 3, it is possible to solve each equation analytically for θ . As is visible in Table 3, the equations of motion for cases 1, 2, and 4 are identical, so these cases will be taken together. Note that they differ only in values of I_o , l_g , and m_b based on the amount of mass added to the pendulum. The value of the damping force b cannot be analytically determined, but it also varies by case.

The equation of motion for cases 1, 2, 3, and 4 is

$$0 = I_o \ddot{\theta} + b\dot{\theta} + l_g m_b g \sin \theta \quad (36)$$

First, we can linearize this equation assuming θ is small (recall that we used a maximum angle of 15° so this is a reasonable estimate). For small θ , $\sin \theta \approx \theta$ and $\cos \theta = \frac{d}{dt} \sin \theta \approx 1$. The equation of motion then becomes:

$$0 = I_o \ddot{\theta} + b\dot{\theta} + l_g m_b g \theta \quad (37)$$

Case 3, whose equation of motion is $0 = I_o \ddot{\theta} + b\dot{\theta} + l_g m_b g \sin \theta + 2k l_b^2 \sin \theta \cos \theta$, linearizes to:

$$0 = I_o \ddot{\theta} + b\dot{\theta} + l_g m_b g \theta + 2k l_b^2 \theta \quad (38)$$

$$0 = I_o \ddot{\theta} + b\dot{\theta} + (l_g m_b g + 2k l_b^2) \theta \quad (39)$$

Equation 39 is the linearized differential equation for case 4. Cases 1-4 are all differential equation of the form $0 = c_1 \ddot{\theta} + c_2 \dot{\theta} + c_3 \theta$. Each case varies only by constants c_1 , c_2 , and c_3 , summarized in the table below using values of I_o and l_g from Table 1:

I will solve the general case for $0 = c_1 \ddot{\theta} + c_2 \dot{\theta} + c_3 \theta$ then substitute in these values for each case at the end. This equation is in its homogeneous form, so there is no need to solve for a particular solution (the particular solution is trivially zero) [2].

First, I can find the natural frequency of the system, ω_n , which is the frequency of the system if damping (the $\dot{\theta}$ term) were not present. In this case, the differential equation is $0 = c_1 \ddot{\theta} + c_3 \theta$. This is a known form of a harmonic oscillator, where the natural frequency is given to be $\omega_n = \sqrt{\frac{c_3}{c_1}}$ [2].

Table 4: Constants c_1 , c_2 , and c_3 Corresponding to Cases 1-4

Case	c_1	c_2	c_3
1	$I_o = \frac{1}{3}m_r l_r^2$	b	$\frac{1}{2}l_r m_r g$
2	$I_o = m_w l_w^2$	b	$l_w m_w g$
3	$I_o = \frac{1}{3}m_r l_r^2 + m_w l_w^2$	b	$l_g(m_r + m_w)g + 2kl_b^2$
4	$I_o = \frac{1}{3}m_r l_r^2 + m_w l_w^2$	b	$l_g(m_r + m_w)g$

Returning back to the case with damping, I will define a variable z , the damping ratio, such that $c_2 = 2c_1 z \omega_n$. Rearranging this, $\frac{c_2}{c_1} = 2z\omega_n$. I can plug this into the differential equation so that:

$$0 = \ddot{\theta} + \frac{c_2}{c_1}\theta + \frac{c_3}{c_1}\theta \quad (40)$$

$$0 = \ddot{\theta} + 2z\omega_n \dot{\theta} + \omega_n^2 \theta \quad (41)$$

Next, it is appropriate to guess a solution of an exponential form with unknown constants A and λ [2]:

$$\theta(t) = Ae^{\lambda t} \quad (42)$$

$$\dot{\theta}(t) = A\lambda e^{\lambda t} \quad (43)$$

$$\ddot{\theta}(t) = A\lambda^2 e^{\lambda t} \quad (44)$$

Substituting these values into the differential equation yields the following:

$$0 = A\lambda^2 e^{\lambda t} + 2z\omega_n A\lambda e^{\lambda t} + \omega_n^2 A e^{\lambda t} \quad (45)$$

$$0 = Ae^{\lambda t} [\lambda^2 + 2z\omega_n \lambda + \omega_n^2] \quad (46)$$

This expression must be zero for all values of t . The term $e^{\lambda t}$ is never zero, while the solution where $A = 0$ is the trivial (equilibrium) solution and is not of interest here. Therefore, the quantity $\lambda^2 + 2z\omega_n \lambda + \omega_n^2$ must be zero to make Equation 46 equal zero. This can be solved using the quadratic formula, and simplified as follows:

$$0 = \lambda^2 + 2z\omega_n \lambda + \omega_n^2 \quad (47)$$

$$\lambda = \frac{-2z\omega_n \pm \sqrt{(2z\omega_n)^2 - 4\omega_n^2}}{2} \quad (48)$$

$$= -z\omega_n \pm \omega_n \sqrt{z^2 - 1} \quad (49)$$

It is often the case that $z^2 - 1$ is negative, so it is convenient to rewrite this solution as follows [2]:

$$\lambda = -z\omega_n \pm \omega_n i \sqrt{1 - z^2} \quad (50)$$

Substituting this result into Equation 42, I obtain a solution for $\theta(t)$:

$$\theta(t) = Ae^{-z\omega_n t \pm \omega_n i \sqrt{1 - z^2} t} \quad (51)$$

This can be rewritten using Euler's identity: $e^{i\theta} = \cos \theta + i \sin \theta$ to obtain the following analytical solution for $\theta(t)$:

$$\theta(t) = e^{-z\omega_n t} (A \cos \omega_n \sqrt{1-z^2} t + B \sin \omega_n \sqrt{1-z^2} t) \quad (52)$$

Because the sine and cosine terms have the same frequency, they can be combined into a single term with a phase shift ϕ , where A and ϕ are unknown:

$$\theta(t) = e^{-z\omega_n t} A \cos (\omega_n \sqrt{1-z^2} t + \phi) \quad (53)$$

Note that the frequency of oscillation of this system is $w_n \sqrt{1-z^2}$, which is called the damped frequency, w_d [2]. This solution can be applied to cases 1-4 to find the analytical solution. Recall the following relationships derived previously:

$$\omega_n = \sqrt{\frac{c_3}{c_1}} \quad (54)$$

$$z = \frac{c_2}{2c_1\omega_n} = \frac{c_2}{2\sqrt{c_1 c_3}} \quad (55)$$

Using these relationships and the expressions for c_1 , c_2 , and c_3 for each case as summarized in Table 1.4.1, the following analytical solutions result for each case:

$$\text{Cases 1 - 4 : } \theta(t) = e^{-\frac{c_2}{2c_1}t} A \cos \left(\sqrt{\frac{c_3}{c_1}} \sqrt{1 - \frac{c_2^2}{4c_1 c_3}} t + \phi \right) \quad (56)$$

Substituting in specific variables from Table 1.4.1, I obtain the following full solutions:

$$\text{Case 1 : } \theta(t) = e^{-\frac{3b}{2m_r l_r^2}t} A \cos \left(\sqrt{\frac{3l_g g}{l_r^2}} \sqrt{1 - \left(\frac{3b^2}{4m_r^2 l_r^2 l_g g} \right)} t + \phi \right) \quad (57)$$

$$\text{Case 2 : } \theta(t) = e^{-\frac{b}{2m_w l_w^2}t} A \cos \left(\sqrt{\frac{g}{l_w}} \sqrt{1 - \left(\frac{b^2}{4l_w^3 m_w^2 g} \right)} t + \phi \right) \quad (58)$$

$$\text{Case 3 : } \theta(t) = e^{-\frac{b}{2(\frac{1}{3}m_r l_r^2 + m_w l_w^2)}t} A \cos \left(\sqrt{\frac{l_g(m_r + m_w)g + 2kl_b}{\frac{1}{3}m_r l_r^2 + m_w l_w^2}} \sqrt{1 - \frac{b^2}{4(\frac{1}{3}m_r l_r^2 + m_w l_w^2)(l_g(m_r + m_w)g + 2kl_b)}} t + \phi \right) \quad (59)$$

$$\text{Case 4 : } \theta(t) = e^{-\frac{b}{2(\frac{1}{3}m_r l_r^2 + m_w l_w^2)}t} A \cos \left(\sqrt{\frac{l_g(m_r + m_w)g}{\frac{1}{3}m_r l_r^2 + m_w l_w^2}} \sqrt{1 - \left(\frac{b^2}{4gl_g(\frac{1}{3}m_r l_r^2 + m_w l_w^2)(m_r + m_w)} \right)} t + \phi \right) \quad (60)$$

These are the full analytical solutions for each case 1-4. Note that there are two unknowns remaining in each Case: A and ϕ . These can be specified using initial conditions if they are given.

1.4.2 Case 5

For case 5, recall that the equation of motion is $kl_b \cos \theta x_o \sin \omega_o t = I_o \ddot{\theta} + b\dot{\theta} + l_g m_b g \sin \theta + 2kl_b^2 \sin \theta \cos \theta$ from Table 3. Using the small angle approximation as was done for cases 1-4, where $\sin \theta \approx \theta$ and $\cos \theta = \frac{d}{dt} \sin \theta \approx 1$, this simplifies to the following:

$$kl_b x_o \sin \omega_o t = I_o \ddot{\theta} + b\dot{\theta} + (l_g m_b g + 2kl_b^2) \theta \quad (61)$$

Table 5: Constants c_1 , c_2 , and c_3 Corresponding to Cases 5

Case	c_1	c_2	c_3
5	$I_o = \frac{1}{3}m_r l_r^2 + m_w l_w^2$	b	$l_g(m_r + m_w)g + 2kl_b^2$

This equation can be written in the form $kl_b x_o \sin \omega_o t = c_1 \ddot{\theta} + c_2 \dot{\theta} + c_3 \theta$ with constants c_1 , c_2 , and c_3 , summarized in the table below:

Note that these values for c_1 , c_2 , and c_3 are identical to those for case 3 derived in the section above.

The solution of the equation of motion for case 5 can be written in terms of a homogeneous solution $\theta_h(t)$ and a particular solution $\theta_p(t)$ where [2]:

$$\theta(t) = \theta_h(t) + \theta_p(t) \quad (62)$$

The homogeneous solution solves the equation $0 = c_1 \ddot{\theta}_h + c_2 \dot{\theta}_h + c_3 \theta_h$. Note again that the constants c_1 , c_2 , and c_3 for case 5 are identical to those for case 3, and the differential equation to be solved is identical as well. Thus, the homogeneous solution for case 5 is given by the full solution for case 3 as expressed in Equations 56 and 59. Repeating these for case 5 below yields the following:

$$\theta_h(t) = e^{-\frac{c_2}{2c_1}t} A \cos \left(\sqrt{\frac{c_3}{c_1}} \sqrt{1 - \frac{c_2^2}{4c_1 c_3}} t + \phi \right) \quad (63)$$

$$= e^{-\frac{b}{2(\frac{1}{3}m_r l_r^2 + m_w l_w^2)}t} A \cos \left(\sqrt{\frac{l_g(m_r + m_w)g + 2kl_b^2}{\frac{1}{3}m_r l_r^2 + m_w l_w^2}} \sqrt{1 - \frac{b^2}{4(\frac{1}{3}m_r l_r^2 + m_w l_w^2)(l_g(m_r + m_w)g + 2kl_b^2)}} t + \phi \right) \quad (64)$$

The particular solution $\theta_p(t)$ solves the following equation [2]:

$$kl_b x_o \sin \omega_o t = c_1 \ddot{\theta}_p + c_2 \dot{\theta}_p + c_3 \theta_p \quad (65)$$

We can assume that the particular solution takes the same form as the forcing term, $kl_b x_o \sin \omega_o t$, which is a sinusoid with frequency ω_o [2]. Therefore, using C and D as undefined constants to be solved for,

$$\theta_p(t) = C \cos \omega_o t + D \sin \omega_o t \quad (66)$$

$$\dot{\theta}_p(t) = -C\omega_o \sin \omega_o t + D\omega_o \cos \omega_o t \quad (67)$$

$$\ddot{\theta}_p(t) = -C\omega_o^2 \cos \omega_o t - D\omega_o^2 \sin \omega_o t \quad (68)$$

Substituting these into the differential equation in Equation 65 yields the following:

$$kl_b x_o \sin \omega_o t = -c_1(C\omega_o^2 \cos \omega_o t + D\omega_o^2 \sin \omega_o t) + c_2(-C\omega_o \sin \omega_o t + D\omega_o \cos \omega_o t) + c_3(C \cos \omega_o t + D \sin \omega_o t) \quad (69)$$

This can be simplified to combine sine and cosine terms as follows:

$$(kl_b x_o + c_1 D\omega_o^2 + c_2 C\omega_o - c_3 D) \sin \omega_o t = (-c_1 C\omega_o^2 + c_2 D\omega_o + c_3 C) \cos \omega_o t \quad (70)$$

The left hand side of the equation must equal the right hand side for all values of t and the equation is of the form $X_1 \sin \omega_o t = X_2 \cos \omega_o t$ where X_1 and X_2 are constants. The only way this is possible

for all values of t is if both X_1 and X_2 are zero. Therefore, the following must be true:

$$0 = kl_b x_o + c_1 D \omega_o^2 + c_2 C \omega_o - c_3 D \quad (71)$$

$$0 = -c_1 C \omega_o^2 + c_2 D \omega_o + c_3 C \quad (72)$$

Solving this system of equations algebraically by combining like terms and solving for constants C and D yields the following result:

$$C = -\frac{kl_b x_o c_2 \omega_o}{(c_3 - c_1 \omega_0^2)^2 + c_2^2 \omega_o^2} \quad (73)$$

$$D = \frac{kl_b x_o (c_3 - c_1 \omega_o^2)}{c_2 \omega_o^2 + (c_3 - c_1 \omega_0^2)^2} \quad (74)$$

The full particular solution is thus the following, using values for c_1 , c_2 , and c_3 as defined in 5:

$$\theta_p(t) = -\left(\frac{kl_b x_o c_2 \omega_o}{(c_3 - c_1 \omega_0^2)^2 + c_2^2 \omega_o^2}\right) \cos \omega_o t + \left(\frac{kl_b x_o (c_3 - c_1 \omega_o^2)}{c_2 \omega_o^2 + (c_3 - c_1 \omega_0^2)^2}\right) \sin \omega_o t \quad (75)$$

The full solution for case 5 using constants c_1 , c_2 , and c_3 as defined in Table 5 is therefore:

$$\text{Case 5 : } \theta(t) = \theta_h(t) + \theta_p(t) \text{ where} \quad (76)$$

$$\theta_h(t) = e^{-\frac{c_2}{2c_1}t} A \sin \left(\sqrt{\frac{c_3}{c_1}} \sqrt{1 - \frac{c_2^2}{4c_1 c_3}} t + \phi \right) \quad (77)$$

$$\theta_p(t) = -\left(\frac{kl_b x_o c_2 \omega_o}{(c_3 - c_1 \omega_0^2)^2 + c_2^2 \omega_o^2}\right) \cos \omega_o t + \left(\frac{kl_b x_o (c_3 - c_1 \omega_o^2)}{c_2 \omega_o^2 + (c_3 - c_1 \omega_0^2)^2}\right) \sin \omega_o t \quad (78)$$

As in cases 1-4, there remain two unknowns in this equation, A and ϕ , which can be solved for given initial conditions. Note that the value of ω_o is not an unknown because it is the frequency at which forcing occurs, which we could set manually using the shaker.

2 Results and Discussion

To analyze the validity of our model, we performed each case and plotted experimental data to compare to the solutions derive above.

2.1 Finding the Spring Constant, k

The first step of data analysis was to find the spring constant of the spring, k . To find this value, we attached a force sensor to one end of the spring and recorded its value for various displacements of the spring, using a ruler. This data is provided in Appendix 3.1. A plot of the data is provided in Figure 15.

As predicted, Figure 15 shows a linear relationship between the spring force F_s and displacement, x . The linearity confirms Hooke's law, which says that the magnitude of the spring force is

$$F_s = -kx \quad (79)$$

where k is the spring constant and x is the displacement of the spring from its natural length. The negative sign indicates that the force operates in the opposite direction of displacement, and can therefore be ignored in the calculation of the spring constant k . Because x and F_s are linearly related by k , the value of k is simply the slope of the line in Figure 15. This value was found to be $k = 48.819$ N/m by taking the slope of the best fit line in the graph.

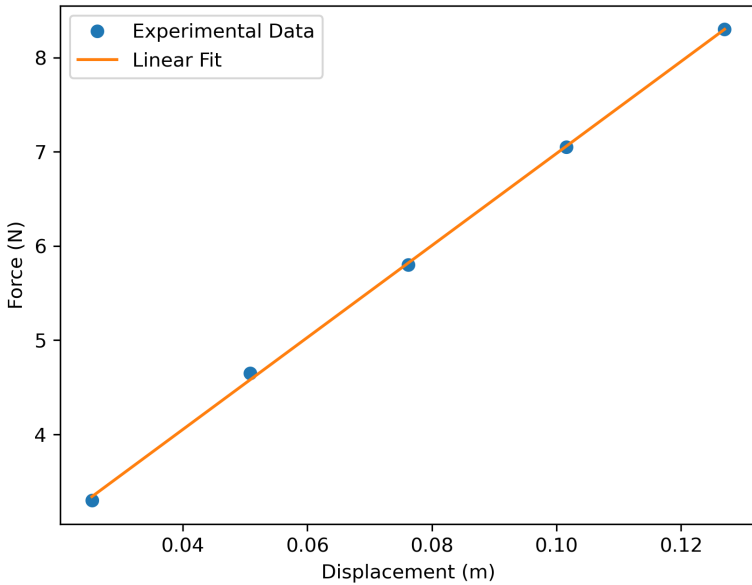


Figure 15: Force vs Displacement for Single Spring

2.2 Experimental Specifications

Having found the value for k , I now have all values needed to solve for numerical solutions of θ vs. time t using the analytical equations derived in the "Solving for Analytical Solutions" section above. Below are the experimental specifications that we measured during data acquisition that we can use to evaluate the analytical solution.

Table 6 gives all the general variables relating to the system as a whole which did not vary by case.

Table 6: Specifications for the Experiment Applicable to All Cases

Pendulum type	k (N/m)	l_c (m)	l_r (m)	l_b (m)	m_r (g)	g (m/s ²)	mass of resin cylinder (g)
3/8 inch steel	48.819	.419	.483	0.318	262.72	9.81	51.38

Other information about the make and model of the equipment is included in the Experimental Setup section of the report.

Table 7 summarizes values that varied by case. I have included in this table variables such as I_o and l_g , which can be solved for using other values in the table and equations derived in the theory section. Note that in finding l_w , the distance from point O to point W , we measured using a ruler to the center of the stack of washers. The washers were assumed to be identical so that their center of mass was located at this point.

Table 7: Specifications for the Experiment Particular to Each Case

Case	m_w (g)	l_w (m)	l_g (m)	I_o (kg·m ²)
1	0	0	.241	.0204
2	106.98	0.457	0.457	.0224
3, 4, 5	57.06	0.457	.280	.0323

2.3 Experimental Results and FFT: Cases 1-4

We took between 15 and 30 seconds of data for each setup in cases 1-4. Before data acquisition, we displaced the pendulum by approximately 15 degrees (measured using a protractor), the released it as we began taking data. In reading the data files, I omitted the first 30 data points recorded because they included considerable noise from the pendulum's release.

Data was initially taken as horizontal displacement y of the pendulum in inches vs. time. I first subtracted the average displacement value from every point on each graph to remove the vertical offset. This enables analysis of the oscillation alone, which is the topic of interest in this lab. I then converted this data into angular displacement θ vs. time by the following formula, where l_c is the distance from point O to the center of the resin cylinder on the rod (this cylinder is the point that the sensor tracks, so this is the appropriate distance to use):

$$\theta(t) = \sin \frac{y(t)}{l_c} \quad (80)$$

This conversion is valid because I assumed small angle approximation where the displacement is perfectly horizontal. This result was used to plot the experimental data as points for angle vs. time in Figures 17 through 20 for each case 1-4.

To find an experimental value for the frequency of the pendulum's oscillation, I fitted a curve to the data we collected. As determined by the analytical solutions, we expect this fit curve to be a sinusoid bounded by an exponentially decaying envelope (see Equation 53). The first task is to find the frequency of the sinusoid, which can be done using a Fast Fourier Transform (FFT).

The Fast Fourier Transform decomposes the data into different frequency sine waves. It then calculates the amount that each sine wave contributes to the overall signal. Figure 16 shows plots of frequency vs. power of the FFT signal as detected by the Fast Fourier Transform algorithm for each case 1-4. Note that the power of the FFT signal is related to the square of the amplitude of the original signal, so its units are radians². The value of this amplitude is not significant for this analysis; we are only interested in the frequency at which the maximum amplitude occurs.

As is visible in the plots, our data has a strong signal around a signal frequency and does not include much noise. Based on these plots, I can expect that the frequencies corresponding to the peak values of amplitude are the oscillating frequency of the pendulum, as these are the frequencies that contribute most to the overall signal. Note that this is the damped frequency w_d , not the natural frequency w_n , since it is derived directly from experimental data. Using NumPy to find this value in each plot, I obtain the following experimental damped frequencies:

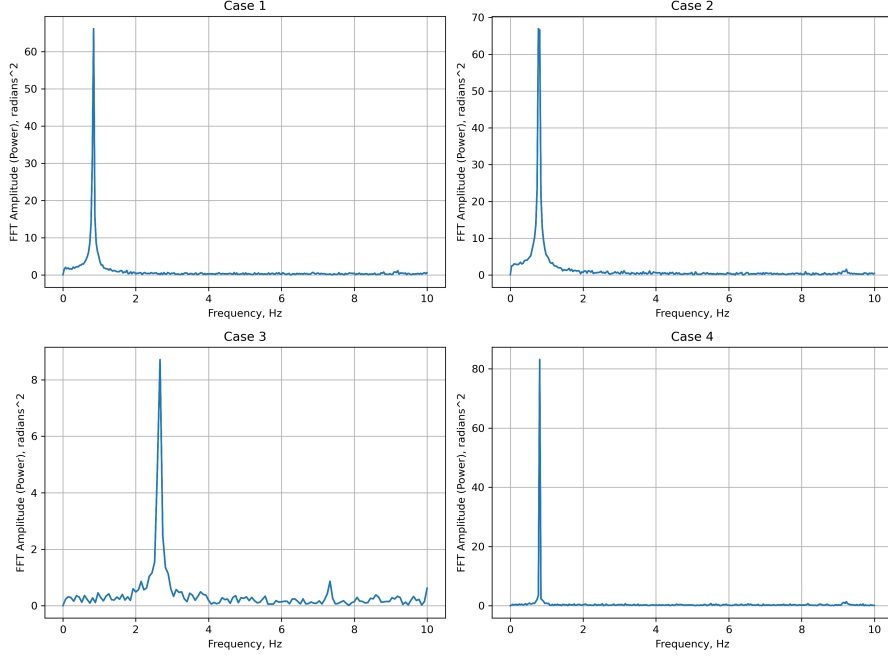


Figure 16: Plots for Cases 1-4 of FFT Frequency vs. Power

Table 8: Experimentally Derived Values for the Damped Frequency, ω_d

	Case 1	Case 2	Case 3	Case 4
Damped Frequency ω_d (Hz)	0.827	0.789	2.641	0.806

2.4 Fitting the Data: Cases 1-4

Now that I have the frequencies of oscillation, I can perform a fitting function using Scipy's curvefit function. This can be used to find the rate of exponential decay of the envelope, from which I can calculate the damping coefficient z . As previously discussed, the fitting function $f(t)$ is of the form:

$$f(t) = Ae^{-qt} \cos(\omega_d t + \phi) \quad (81)$$

because we expect it should take the same form as the analytical solutions derived in the Theory section (see Equation 53). Note that I did not include a vertical shift term because I removed the vertical offset from the plot as one of the initial steps of data analysis.

In Equation 81, A , q , and ϕ are parameters to be determined by the fitting algorithm. Recall that ω_d was already determined using FFT analysis. The algorithm requires inputting initial conditions for each of these parameters. Initial conditions were determined as follows:

- A : This is the initial amplitude of the function and was estimated from a visual inspection.
- q : This is the exponential decay term. From visual inspection, this is small so I guessed 0.2.
- ϕ : This is the initial phase shift. This was estimated to be zero in each case, since we released the pendulum from a position of maximum amplitude.

The initial guesses used are presented below in Table 9:

Table 9: Initial Guesses Used for Scipy's Curvefit Function

Case	A (radians)	q	ϕ (radians)
1	0.381	0.2	0
2	0.369	0.2	0
3	0.083	0.2	0
4	0.293	0.2	0

After running the algorithm on the experimental data using these initial conditions, I received the following values for the fitted constants:

Table 10: Fitted Parameters Found Using for Scipy's Curvefit Function

Case	A (radians)	q	ϕ (radians)
1	0.4196	.0064	2.3398
2	-0.3934	0.0042	-0.0252
3	0.1270	0.0628	2.5130
4	-0.3121	0.0042	-0.1841

This function determines q , related to the system parameter for damping. Comparing the form of the fitted function in Equation 81 to the analytical solution in Equation 52 shows that:

$$q = z\omega_n = \frac{b}{2I_o} \quad (82)$$

As discussed in Equation 52, the conversion from damped frequency to natural frequency is:

$$w_d = w_n \sqrt{z^2 - 1} \quad (83)$$

The values for q are given in the tables above, while the damped frequency w_d was determined in Table 8 using the Fast Fourier Transform. Therefore, I have two equations and two unknowns and can solve between them to obtain the experimental natural frequency as follows:

$$\omega_n = \sqrt{q^2 + \omega_d^2} \quad (84)$$

Using this relationship, I can find the experimental natural frequency as well as the damping coefficient z where

$$z = \frac{q}{\omega_n} \quad (85)$$

These values are included in Table 11 below alongside the damped frequencies found earlier for comparison.

Table 11: Derived Experimental Parameters for Cases 1-4

Case	Damped Frequency w_d (Hz)	Natural Frequency w_n (Hz)	Damping Coefficient z
1	0.8273	0.8273	0.0012
2	0.7370	0.7895	0.0008
3	2.6414	2.6414	0.0038
4	0.8058	0.8058	0.0008

Note that the values of z are so small in each case that they barely affect the frequency of oscillation.

Given the experimentally determined values for ω_n and z , I can plot the analytical solution of the exponential decay envelope of the form

$$f(t) = Ae^{-\omega_n z t} \quad (86)$$

The parameter A models the initial amplitude of the oscillation and was determined using the fitting function (see Table 11), and ω_n and z are determined above in the discussion just above. Using these, I have plotted the analytical prediction alongside the experimental data for each case in Figures 17 to 20. Additionally, I have included plots with the full analytical solution including the sinusoidal motion in the appendix.

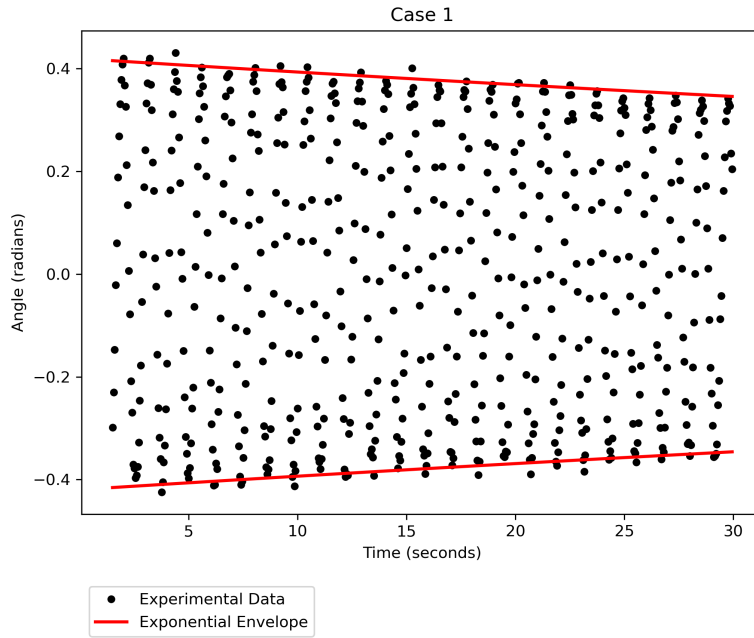


Figure 17: Experimental Data and Analytical Solutions with Decay Envelope: Case 1

Using Figures 17 to 20 as a reference, the analytical model of the form $Ae^{-qt} \cos(\omega_d + \phi)$ was a very close match to the data in all four cases. Case 1 had a particularly close match, with

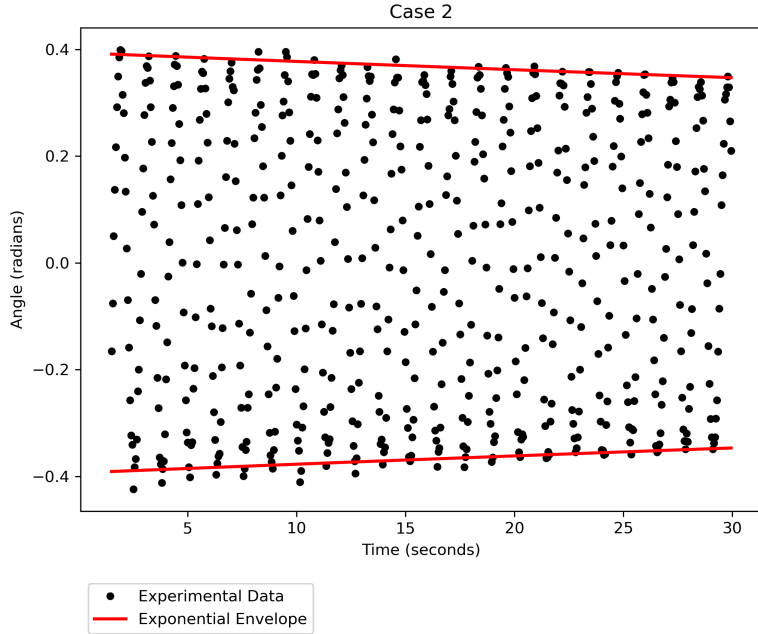


Figure 18: Experimental Data and Analytical Solutions with Decay Envelope: Case 2

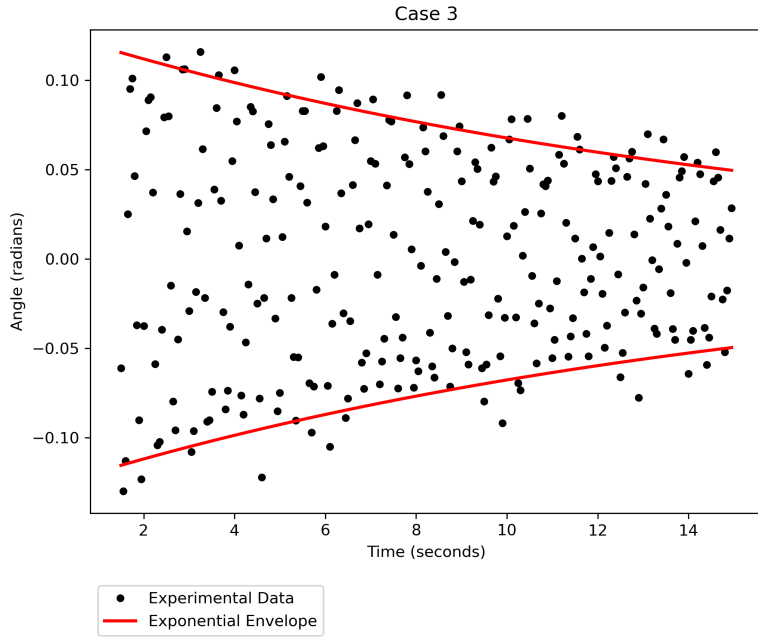


Figure 19: Experimental Data and Analytical Solutions with Decay Envelope: Case 3

only eight experimental data points falling outside the fitted function's path. Case 3 had the least accurate fit, as many experimental data points fell outside the exponential decay envelope. This

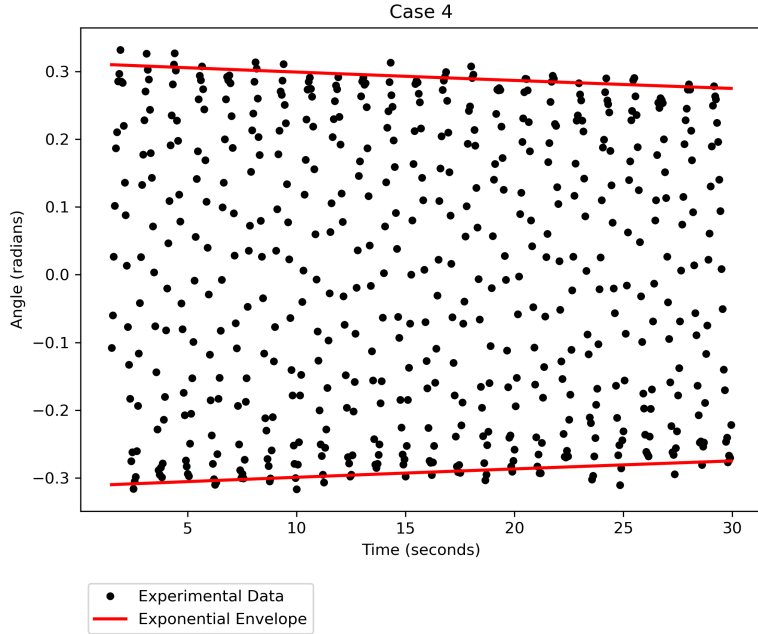


Figure 20: Experimental Data and Analytical Solutions with Decay Envelope: Case 4

is likely because the data for this case was taken during the first week of experiments, when there were slight issues with calibration on the 3/8 inch steel pendulum setup. We discarded our data from the first week for cases 1, 2, and 4 and collected new data the second week, but we elected to keep our original data for case 3 because it appeared to be regular. Another reason for this discrepancy could be the presence of the springs, which added extra parameters to the system and therefore more sources of experimental uncertainty. For instance, the springs are not perfectly ideal and could produce different force in compression than in tension, causing slight fluctuations in the pendulum's amplitude between oscillations. Other systemic errors and sources of uncertainty for all cases were also present and are considered further in the discussion that follows.

2.5 Comparison of Analytical and Experimental Data

The section above derives natural frequency ω_n , damped frequency ω_d , and the damping coefficient z from experimental data for each case 1-4. I can also solve independently for analytical values for these variables. To find the natural frequency ω_n analytically, I can use the relationship from Equation 54 that

$$\omega_n = \sqrt{\frac{c_3}{c_1}} \quad (87)$$

Using expressions for c_3 and c_1 from Table 1.4.1 and system parameters from Table 7, I obtain natural frequencies for each case which are presented in Table 12.

Using the value obtained for z derived experimentally I can solve for the analytical damped frequency using the following relationship derived in Equation 83:

$$\omega_d = \omega_n \sqrt{z^2 - 1} \quad (88)$$

Finally, I can find an analytical solution for the damping coefficient b by using the following relationship from Equation 40 and the experimentally derived value for z :

$$b = 2z\omega_n I_o \quad (89)$$

These parameters for the analytical solutions are summarized in Table 12 below.

Table 12: Derived Analytical Parameters for Cases 1-4

Case	Damped Frequency w_d (Hz)	Natural Frequency ω_n (Hz)	Damping Coefficient b
1	0.8788	0.8788	0.0003
2	0.7372	0.7372	0.0002
3	2.8984	2.8984	0.0045
4	0.8294	0.8294	0.0003

Using Table 11 for the experimentally derived values, the analytically and experimentally derived parameters for natural frequency are compared and summarized below in Table 13.

Table 13: Comparison of Experimental and Analytical Natural Frequencies

Case	Experimental Frequency ω_n (Hz)	Analytical Frequency ω_n (Hz)	Percent Error
1	0.8273	0.8788	6.225
2	0.7895	0.7372	6.619
3	2.6414	2.8984	9.733
4	0.8058	0.8294	2.930

The last column includes percent error of the analytical frequency as compared to the experimental frequency, calculated as follows:

$$\% \text{ error} = \frac{|\text{Analytical } \omega_n - \text{Experimental } \omega_n|}{\text{Experimental } \omega_n} \times 100 \quad (90)$$

The frequencies obtained experimentally closely match the frequencies expected based on our analytical model, indicating the validity of our model. A further discussion on the comparison and possible sources of error are included in the following section.

2.6 Discussion and Sources of Error: Cases 1-4

The quality of my mathematical model can be analyzed by making comparisons with the experimental data using values from 13 and the plots in Figures 17 through 20.

In terms of experimentally vs. analytically derived values for natural frequencies as presented in Table 13, in each case, the experimental and predicted values make sense based on the weights, spring stiffness, and other specifications for the experiment. This is evident as the percent error for the analytical frequency as compared to the experimental frequency is small in all cases. Similarly,

as discussed previously, the analytical solution of the decay envelope from Figures 17 through 20 matches the data closely in all cases as well, indicating the mathematical models are relatively accurate. The model predicted underdamped oscillation with an exponential decay envelope, which matched the observed experimental result.

The analytical frequencies found in cases 1, 2, and 4 were higher than the experimental frequencies for those cases. Lower frequency indicates a slower rate of movement. This suggests there may have been additional sources of damping present in the experiment that were not accounted for in our model, such as air drag, which caused the frequency of oscillation to be lower than we predicted. Additionally, the presence of the resin cylinder on the rod caused the center of mass to be slightly further down the rod than our model predicted. This could cause a larger moment of inertia and therefore a smaller frequency measurement (recall that $\omega_n = \sqrt{\frac{c_3}{c_1}}$, where c_1 is the moment of inertia about point O, I_o . Therefore, increasing I_o causes ω_n to decrease). In case 2, this had the opposite effect. In this case, we neglected the mass of the rod and the resin cylinder, so the true center of mass of the system was closer to point O than our model predicted. This causes the analytical value of I_o to be larger than it is in reality, which in turn produces an analytical frequency that is lower than the true experimental value.

Of the four cases, cases 1, 2 and 4 were the closest matches in both Table 13 and Figures 17 through 20. This is likely because the mathematical models for these cases most closely described the true experimental setup. In case 1, the system was modelled as a slender rod of uniform mass, which almost exactly describes the real experiment. The presence of the resin cylinder meant the true center of mass was lower on the rod than we modelled it to be, as described above, but otherwise the system was extremely simple so there were fewer simplifications I had to make in my modelling decisions.

Similarly, system 2 was modelled as a point particle of mass m_w , neglecting the mass of the rod and resin cylinder. This was a reasonable assumption because the mass is heavy enough to significantly affect the center of mass and can be modelled alone without greatly affecting the obtained results. Because of this, the analytical prediction matches the true observed result very closely. As described above, though, the analytical prediction for this case is unique in that it is lower than the experimental result due to neglecting the rod's mass.

The analytical prediction of ω_n for case 4 was also a very close match to the experimental frequency, with a percent error of only 2.930%. This case matched extremely closely because I modelled the system as rod plus a point mass attached together. Because this model accounted for the rod's mass, it was more accurate than the prediction for Case 2. Furthermore, it is more accurate than Case 1 because the added point mass means the resin cylinder comprises a smaller percentage of the total mass of the system. Therefore, neglecting its mass in the model has a smaller effect on the overall result.

Case 3 has the largest error, although at only 9.733% error for w_n , it is still a very good match. Its analytically modelled envelope of decay in Figure 19 is also the least precise of the four setups. Aside from the springs, this system was modelled exactly like Case 4, which had the smallest percent error. Thus, it is reasonable to assume that systematic errors in modelling the springs is the main source of error for this case. One possible reason is that I modelled the spring force on the rod from each spring as $F_s = -kx$, where F_s is the spring force, k is the spring constant, and x is the displacement of the spring from the $\theta = 0$ position. I modelled the total spring force on the rod as $2F_s$, assuming the force of each spring on the rod was equal. However, this assumption is not perfect because the springs likely did not have the same force in tension as in compression, which is assumed for ideal springs. From manual inspection, the springs appeared to have a larger spring constant in tension than in compression (in fact, the lab manual mentions they are "tension

springs") [1]. This caused a larger standard deviation in the amplitude of oscillation, as is visible in Figure 19. Accounting for only the tension in the spring would have resulted in a more accurate mathematical model. Furthermore, the displacement for each of the springs is not exactly equal at any given time. Since the rod has a diameter, the true displacement of the springs should technically vary by 3/8 inches inches. It is also possible that using the small angle approximation in this model negatively affected our prediction, as we released the spring from 15°, which is on the upper limit of the accepted range for small angle approximation. Adjusting the model to account for these errors would have likely resulted in a smaller error for this case.

Note that as is shown in the data from in Table 12, the value of damped frequency and natural frequency for each case is extremely close, especially for cases 1, 2, and 4. This is because the damping ratio z is very small, so it does not have a large effect on the observed frequency of oscillation. The source of drag that we modelled mathematically occurred at the pin, so the most likely cause of this is friction at this point. The pendulum setup was attached to the metal cage using a roller bearing, which minimizes friction, explaining why the damping effect was minimal. For case 3, the springs also had an effect on the decay of the slope. Though they are conservative forces and do not cause a decrease in the system's overall energy, they did affect the rate of amplitude decay. Their contribution increases the damping coefficient, as is seen by the larger exponential decay rate in Figure 19.

2.7 Results and Discussion: Case 5

For the fifth case, the springs were attached to the rod and a horizontal sinusoidal forcing frequency ω_o was imposed on one of the springs. We collected data on the rod's displacement for a range of twenty different frequencies between 1Hz and 5Hz. I can use the same relationship established in Equation 80 to translate this data into angular displacement of the rod:

$$\theta(t) = \sin \frac{x(t)}{L} \quad (91)$$

I used this data to plot angular displacement as a function of time for each of the twenty data sets in Figure 21. This plot helps to visualize each dataset and understand the behavior of how the system responds to different frequencies.

Recall that the homogeneous solution to this case is exactly the same as that for Case 3, and is expressed in Equation 59. Therefore, the expected experimentally and analytically derived frequencies based on system parameters is the same as in Case 3. From Table 12, I find the following:

$$\text{Case 5, Experimental : } \omega_n = 2.645\text{Hz} \quad (92)$$

$$\text{Case 5, Analytical : } \omega_n = 2.898\text{Hz} \quad (93)$$

The experimentally determined natural frequency is more representative of the true natural frequency because it was derived directly from the data, so I will use this value in the discussion for case 5.

As Figure 21 shows, the system response near the experimental resonance frequency of 2.645 Hz have higher do not have oscillating "beats" resulting from interfering sinusoidal responses from the system. Rather, as is visible in the plots for a forcing frequency of 2.6 Hz and 2.7Hz, the amplitude is constant with time because the forcing frequency matches the natural frequency of the system, and their signals add constructively. For very high values and very low values of forcing frequency, we expect the steady state response of the system to be almost completely due to the

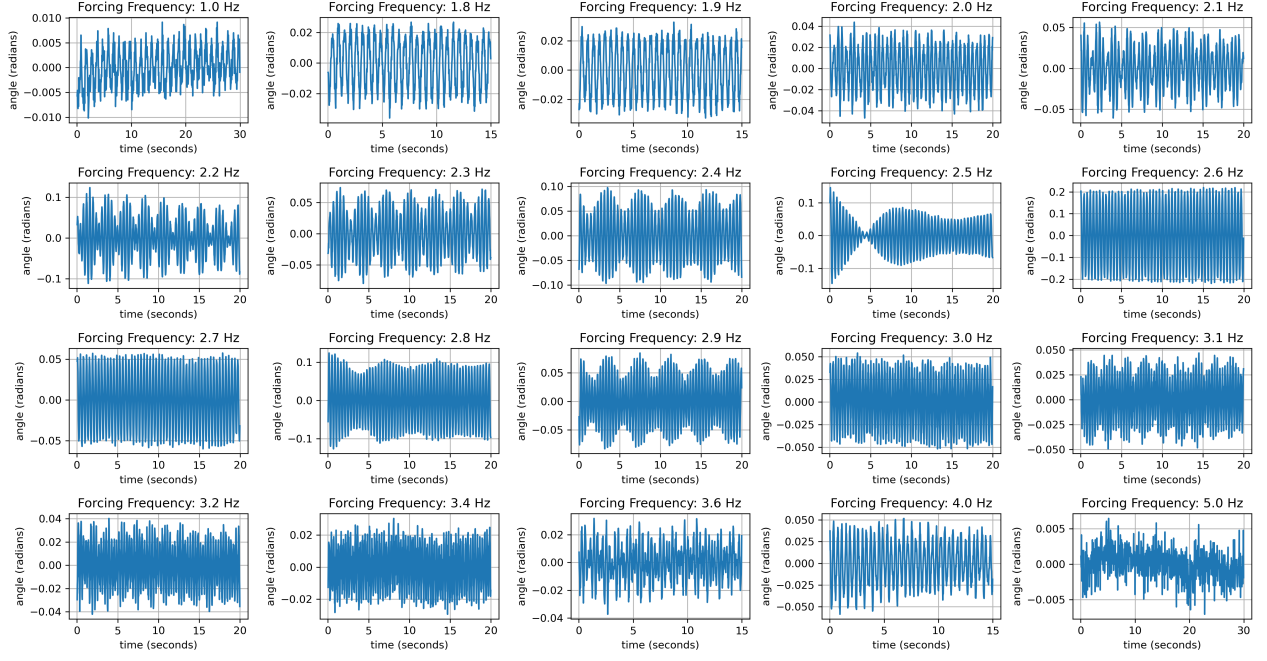


Figure 21: Experimental Angular Displacement vs. Time for a Range of Forcing Frequencies

forcing frequency and have very little contribution from the natural frequency. This is qualitatively visible in the first and last plots in 21: for a forcing frequency of 1.0 Hz, the frequency of oscillation appears to be much larger (in fact, approximately 5 times as large) as that for the forcing frequency of 5Hz. The period of oscillation for the 1.0 Hz case looks to be about 1s, which corresponds to a 1.0Hz frequency of oscillation, whereas the oscillations are much faster for the 5Hz case.

To further this analysis, it is useful to quantitatively analyze the amplitude of the system's steady state response as a function of forcing frequency. I found the amplitude of each plot by finding the maximum value in each plot after it had reached steady state (I took the maximum value after 10 seconds, after which all cases appear to be in steady state). Using these values, I plotted the amplitude of the system's steady state response as a function of the forcing frequency in Figure 22.

As this plot shows, the amplitude of oscillation peaks is at 2.6 Hz, which is nearest to the expected frequency of 2.645 Hz. This amplitude is not infinite because the system includes damping. The amplitude generally decreases in either direction as the amount of constructive interference between the natural frequency and forcing frequency decreases. For cases with very small and very large forcing frequencies, the amplitude of oscillation is very small. This is because the steady state oscillation in these cases results almost completely due to the forcing frequency rather than the natural frequency. Because the amplitude of the shaker's motion was very small, the amplitude of the system's response is very small as well.

Note that the amplitudes at 2.7 Hz and 2.3 Hz are smaller than would be expected by the general shape of the graph. This is likely because the signal varies large amounts near the forcing frequency. It is possible that the natural and forcing frequency interfered destructively for the period of time that we took measurements, resulting in a smaller amplitude than expected.

Overall, the data fits the expected shape, confirming the result from case 3 that the natural frequency of the system is 2.645 Hz. However, the shape is not perfect and we could gain more

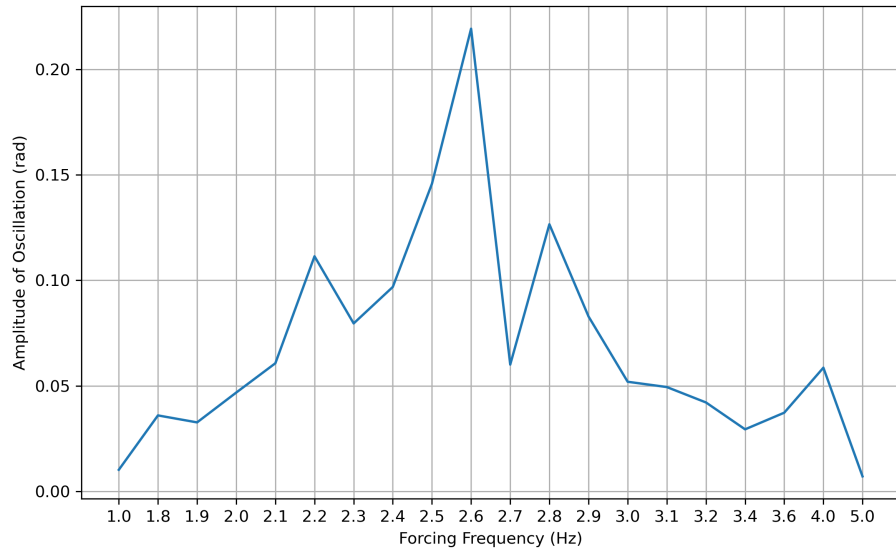


Figure 22: Amplitude of Oscillation vs. Forcing Frequency

insight by increasing the time of data acquisition as well as the number of forcing frequencies tested.

References

- [1] Santillan, Sophia. "Laboratory 2: Underdamped, Free/Driven Oscillator Manual." EGR 244L Dynamics. 20 Mar. 2023, Duke University.
- [2] Santillan, Sophia. "Lecture on Damped Oscillators." EGR 244 Lectures. 6 Apr. 2023, Duke University.
- [3] Santillan, Sophia. "Lecture on Lagrange's Method." EGR 244 Lectures. 28 Mar. 2023, Duke University.
- [4] Santillan, Sophia. "Lecture on Work Energy Approach for Rigid Bodies." EGR 244 Lectures. 7 Mar. 2023, Duke University.
- [5] Kasdin, N. Jeremy, and Derek A. Paley. Engineering Dynamics: A Comprehensive Introduction. Princeton University Press, 2011.

3 Appendix

3.1 Data for Spring Force vs. Displacement

```
1 disp  force_N
2 .0254 3.3
3 .0508 4.65
4 .0762 5.8
5 .1016 7.05
6 .127 8.3
```

3.2 Plots of Analytical Prediction with Fitted Sinusoid

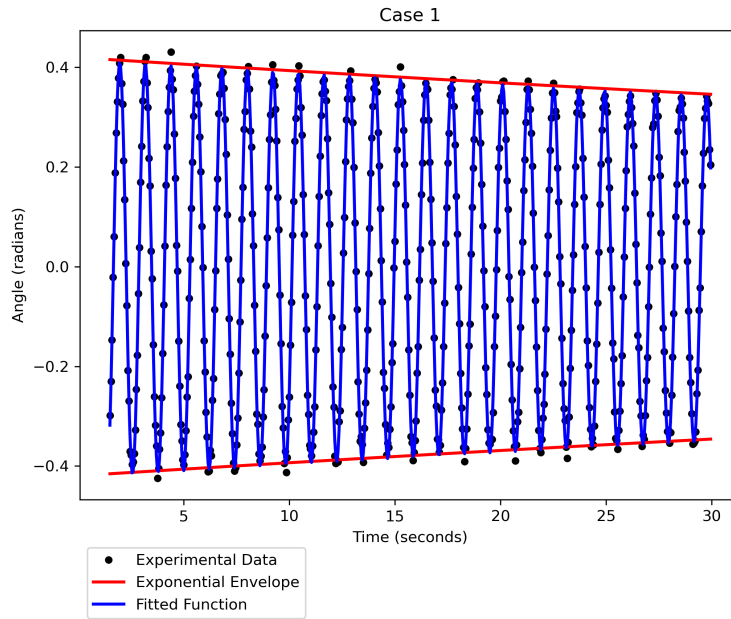


Figure 23: Experimental Data and Analytical Solutions with Decay Envelope: Case 1

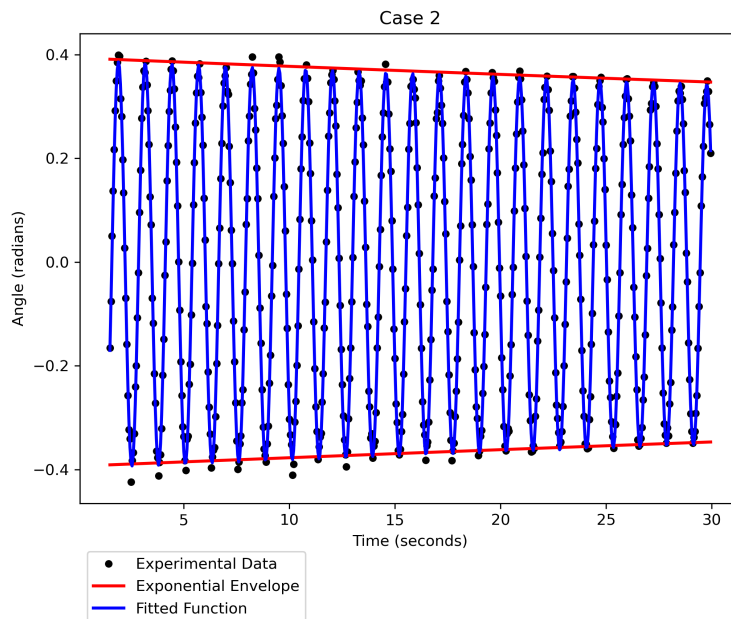


Figure 24: Experimental Data and Analytical Solutions with Decay Envelope: Case 2

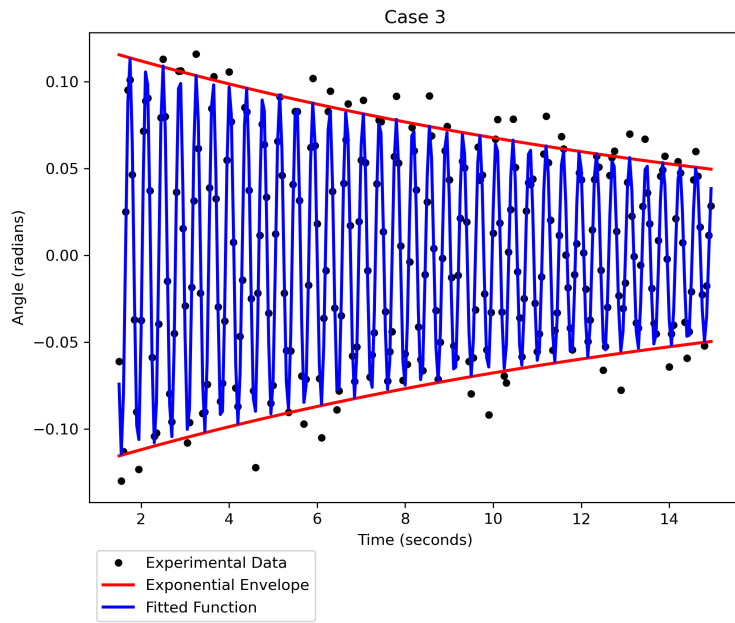


Figure 25: Experimental Data and Analytical Solutions with Decay Envelope: Case 3

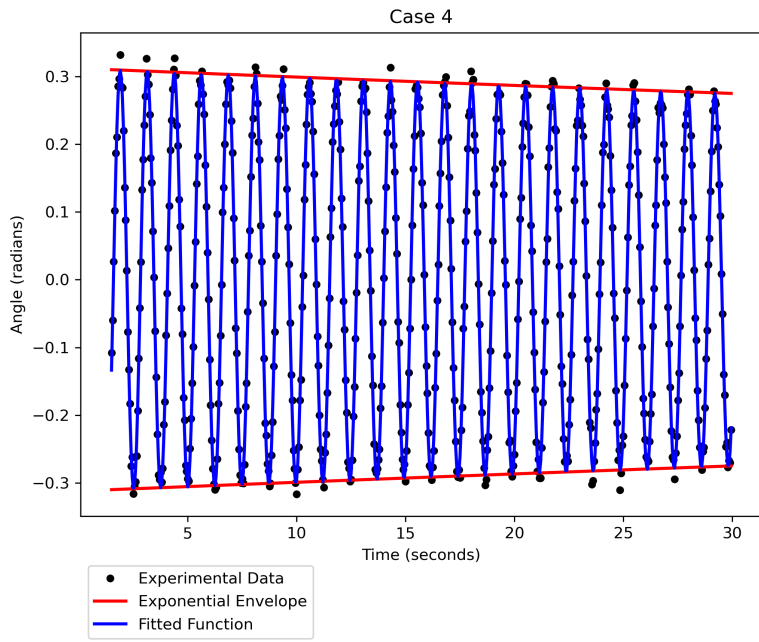


Figure 26: Experimental Data and Analytical Solutions with Decay Envelope: Case 4

3.3 Code

```
1 """
2 Created on Tue Mar 21 13:45:39 2023
3
4 @author: lizzyjones
5 """
6
7 import os
8 import numpy as np
9 import matplotlib.pyplot as plt
10 import imageio
11 import glob
12 import pandas as pd
13
14 from scipy.optimize import curve_fit
15 from scipy.signal import butter, filtfilt
16 from scipy.fft import fft, fftfreq
17 from numpy.lib import stride_tricks
18
19 #%% import data
20
21 # data for spring constant
22 k_file = 'force_vs_disp_data.txt'
23 k_data = pd.read_table(k_file)
24
25 # data for experiments 1-4
26 file_names = sorted(glob.glob('setup*.csv'))
27 all_data = []
28 for file_name in file_names:
29     data = pd.read_csv(file_name, names=['time', 'dist'], skiprows=30)
30     all_data.append(data)
31
32 set1_t1_d2, set1_t2_d2, set1_t1, set1_t2, set1_t3, set2_t1, set2_d2, set2_t2,
33     set3_t1, set3_t2, set3_t3, set4_d2, set4_t1, set4_t2, set4_t3 = all_data
34 #samples = np.load(file_paths)
35
36 # data for shaker experiment
37 shaker_files = sorted(glob.glob('*.*.csv'))
38 shaker_data = []
39 for file_name in shaker_files:
40     data = pd.read_csv(file_name, names=['time', 'dist'], skiprows=1)
41     shaker_data.append(data)
42
43 #%% calculating spring constant
44 disp = np.asarray(k_data['disp'])                      # displacement in m
45 force = np.asarray(k_data['force_N'])                  # force in N
46
47
48 p_for_k = np.polyfit(disp, force, 1)
49 disp_model = np.linspace(disp.min(), disp.max())
50 force_model = np.polyval(p_for_k, disp_model)
51
52 fig, ax= plt.subplots(1,1)
53 ax.plot(disp, force, 'o', label="Experimental Data")
54 ax.plot(disp_model, force_model, label = 'Linear Fit')
55 ax.legend()
56 ax.set(xlabel='Displacement (m)', ylabel="Force (N)")
```

```

57 fig.savefig('spring_force_vs_disp.png', dpi=300)
58
59 k3 = p_for_k[0] # spring constant for model 3
60 print('spring constant: {} N/m'.format(k3))
61
62 #%% fft
63
64 x_plot = []
65 y_plot = []
66
67 def fit_fn(df):
68     t = np.asarray(df['time'])
69     raw_sig = np.asarray(df['dist']) #in inches
70     no_offset_sig = raw_sig - raw_sig.mean() # removes dc component (shift)
71     sig = np.arcsin(no_offset_sig/(np.ones_like(no_offset_sig)*L)) # uses angles
72
73     ff = fftfreq(len(t), t[1]-t[0]) # assumes uniform time spacing, computes bins
    for frequency
74
75     Fyy = abs(fft(sig))
76
77     x_plot.append(np.abs(ff))
78     y_plot.append(np.abs(Fyy))
79
80     #fig = plt.figure()
81     #ax = fig.add_subplot()
82     #ax.plot(np.abs(ff), np.abs(Fyy))
83     #ax.set(xlabel='Frequency (Hz)', ylabel='FFT Amplitude')
84
85     f_idx = np.argmax(Fyy)
86     f = ff[f_idx]
87     w = f*np.pi*2
88     A = np.sqrt(np.max(Fyy))
89     p = np.angle(fft(sig)[f_idx]) #phase shift angle
90
91     fps = 1/(t[1]-t[0]) # Hz
92
93
94     guess_freq = abs(ff[np.argmax(Fyy[1:])+1]) # excluding the zero frequency
    "peak", which is related to offset
95     guess_amp = np.std(sig) * 2.***0.5 # gives spectral density
96     guess_offset = np.mean(sig)
97     guess = np.array([guess_amp, .2, 2.*np.pi*guess_freq, 0., guess_offset])
98
99     def sinfunc(t, A, k, w, p, c): return A * np.exp(-k*t)*np.cos(w*t + p) + c
100    popt, pcov = curve_fit(sinfunc, t, sig, p0=guess)
101    A, k, w, p, c = popt
102    f = w/(2.*np.pi)
103    fitfunc = lambda t: A * np.exp(-k*t) * np.cos(w*t + p) + c
104    expfunc = lambda t: A * np.exp(-k*t)
105    print("A", A)
106    print("q", k)
107    print("p", p)
108    print("c", c)
109
110    return {"amp": A, "omega": w, 'exponent': k, "phase": p, "offset": c, "freq": f,
    "period": 1./f, "fitfunc": fitfunc, "expfunc": expfunc, "maxcov": np.max(
    pcov), "rawres": (guess,popt,pcov)}

```

```

112
113 L = 16.5 #use inches because distance array is in inches
114
115 t_list = []
116 angles_list = []
117 fft_dists_list = []
118 models=[]
119 for dataset in all_data:
120     t = np.asarray(dataset['time'])
121     dists = dataset['dist']-np.mean(dataset['dist'])
122     angles = np.arcsin(dists/(np.ones_like(dists)*L))
123
124     model = fit_fn(dataset)
125     models.append(model)
126
127     t_list.append(t)
128     angles_list.append(angles)
129
130 use_indices = [1, 5, 10, 11]
131
132 # experimental omega values
133 def get_w(idx):
134     return models[use_indices[idx]]['omega']
135
136 # damped freq!! find the natural from this
137 expt_w = np.array([get_w(0), get_w(1), get_w(2), get_w(3)])
138 expt_f = expt_w/(2*np.pi)
139
140
141 #%% analytical for first 4 setups
142
143 mr = 262.72/1000*np.array([1,0,1,1]) # kg; mass of
144     rod
145 mw = np.array([0, 106.98, 57.06, 57.06])/1000 # kg; mass added
146 lr = np.array([19*.0254, 0, 19*.0254, 19*.0254])
147     # m; length of rod
148 lw = np.array([17.5, 18, 18, 18])*0.0254 # m; distance to mass; varies by
149     expt
150 lb = 12.5*.0254 # m; distance to springs
151 attachment
152 ls = 16.5*.0254 # m; distance to the resin
153 cylinder/sensor
154 g = 9.81 # m/s^2; gravity
155 k = np.array([0, 0, k3, 0]) # N/m; spring constant (zero for
156     cases 1, 2, 4)
157
158 m_tot = mr+mw
159
160 def get_b(idx):
161     return models[use_indices[idx]]['exponent']
162 b = np.array([get_b(0), get_b(1), get_b(2), get_b(3)])
163
164 lg = (.5*lr*mr + lw*mw)/(mr+mw) # distance from O to G
165 Io = (1/12)*mr*(lr**2) + mr*(.5*lr)**2 + mw*(lw)**2 # moment of inertia around O
166 wn = np.sqrt((m_tot*g*lg + 2*k*lb**2)/Io) # analytical nat freq
167 nat_freq = wn/(2*np.pi)
168
169 z = b/(2*Io*wn)

```

```

165 damp_ratio = np.sqrt(1-z**2)
166 wd = wn*(damp_ratio)
167
168 damped_freq = wd/(2*np.pi)                                #analytical damped freq
169
170 expt_wn = expt_w/np.sqrt(1-z**2)
171 expt_fn = expt_wn/(2*np.pi)
172
173 def analytical_model(model_index, damped_freq):
174     # print(model_index)
175     # print('amp', models[model_index]["amp"])
176     # print('freq', damped_freq)
177     print('exp', models[model_index]["exponent"])
178
179     return models[model_index]["amp"]* np.exp(-models[model_index]["exponent"]*t_list[model_index]) * np.sin(damped_freq*t_list[model_index] + models[model_index]["phase"]) + models[model_index]["offset"]
180
181 freq_error = np.abs(expt_fn-nat_freq)/expt_fn*100
182
183 #%% plots for scenarios 1-4
184 ''
185 fig, axs = plt.subplots(nrows=2, ncols=2, )
186
187 count=0
188 for ax, index in zip(axs.ravel(), use_indices):
189     #if count ==2: l = -1
190     #else: l=1
191     ax.plot(t_list[index], angles_list[index], 'k-', markersize=1)
192     ax.plot(t_list[index], angles_list[index], 'ko', markersize=3, label='Experimental Data')
193     ax.plot(t_list[index], -models[index]["expfunc"](t_list[index]), "r-", linewidth=2)
194     ax.plot(t_list[index], models[index]["expfunc"](t_list[index]), "r-", linewidth=2)
195     ax.plot(t_list[index], analytical_model(index, wd[count]), 'r-', label="Analytical Solution")
196     #ax.plot(t_list[index], models[index]["fitfunc"](t_list[index]), "r-", label="y fit curve", linewidth=2)
197     ax.set(xlabel='time (seconds)', ylabel='angle (radians)', title = 'Case {}'.format(count+1))
198
199     ax.grid()
200     count+=1
201
202 fig.legend(bbox_to_anchor=(-5, 0))
203 fig.tight_layout()
204 ''
205 #%%
206
207 count=0
208 for index in use_indices:
209     #if count ==2: l = -1
210     #else: l=1
211     fig, ax = plt.subplots(1,1, figsize=(7,6))
212     #ax.plot(t_list[index], angles_list[index], 'b-', markersize=1, label='Fitted Function')
213     ax.plot(t_list[index], angles_list[index], 'ko', markersize=4, label='Experimental Data')

```

```

214     ax.plot(t_list[index], -models[index]["expfunc"](t_list[index]), "r-", linewidth=2, label='Exponential Envelope')
215     ax.plot(t_list[index], models[index]["expfunc"](t_list[index]), "r-", linewidth=2)
216     #ax.plot(t_list[index], analytical_model(index, wd[count]), 'r-', label="Fitted Function")
217     ax.plot(t_list[index], models[index]["fitfunc"](t_list[index]), "b-", linewidth=2, label="Fitted Function", linewidth=2)
218     ax.set(xlabel='Time (seconds)', ylabel='Angle (radians)', title = 'Case {}'.format(count+1))
219     plt.legend(bbox_to_anchor =(0,-0.27), loc='lower left')
220     fig.tight_layout()
221     fig.savefig('analytical_and_exptl_{}.png'.format(count+1), dpi=300)
222
223     ax.grid()
224     count+=1
225
226 #%% shaker experiment
227
228 for df in shaker_data:
229     raw_sig = np.asarray(df['dist'])
230     no_offset_sig = raw_sig - raw_sig.mean() # removes dc component (shift)
231     sig = np.arcsin(no_offset_sig/(np.ones_like(no_offset_sig)*L)) # uses angles
232     df['sig'] = sig
233
234 fig, axs = plt.subplots(nrows=4, ncols=5, figsize=(17,10))
235 for ax, index in zip(axs.ravel(), np.arange(len(shaker_data))):
236     ax.plot(shaker_data[index]['time'], shaker_data[index]['sig'])
237     ax.set(xlabel='time (seconds)', ylabel='angle (radians)', title = 'Forcing Frequency: {} Hz'.format(shaker_files[index][:3]))
238     ax.grid()
239
240 fig.tight_layout()
241 fig.savefig("case_5.png", dpi=300)
242
243 #%
244 #shaker amplitude
245
246 freqs = []
247 amps = []
248 for index in np.arange(len(shaker_data)):
249     min_pt = shaker_data[index]['sig'][200:].min()
250     freq = shaker_files[index][:3]
251     freqs.append(freq)
252     amps.append(np.abs(min_pt))
253
254 fig = plt.figure(figsize=(8,5))
255 ax = fig.add_subplot()
256 ax.plot(freqs, amps)
257 ax.set(xlabel='Forcing Frequency (Hz)', ylabel='Amplitude of Oscillation (rad)')
258 ax.grid()
259 fig.tight_layout()
260 fig.savefig('amps_vs_freq.png', dpi=300)
261
262 #%% make FFT plots for report
263
264 use_indices = [1, 5, 10, 11]
265 for index in use_indices:
266     fit_fn(all_data[index])

```

```
267 fig, axs = plt.subplots(nrows=2, ncols=2, figsize=(12,10))
268 count=1
269 for ax, index in zip(axs.ravel(), [0,5,10,11]):
270     ax.plot(x_plot[index], y_plot[index])
271     ax.set(xlabel='Frequency, Hz', ylabel='FFT Amplitude (Power), radians^2',
272            title = 'Case {}'.format(count))
273     ax.grid()
274     count+=1
275
276 fig.tight_layout()
277 fig.savefig('FFT_example.png', dpi=300)
```